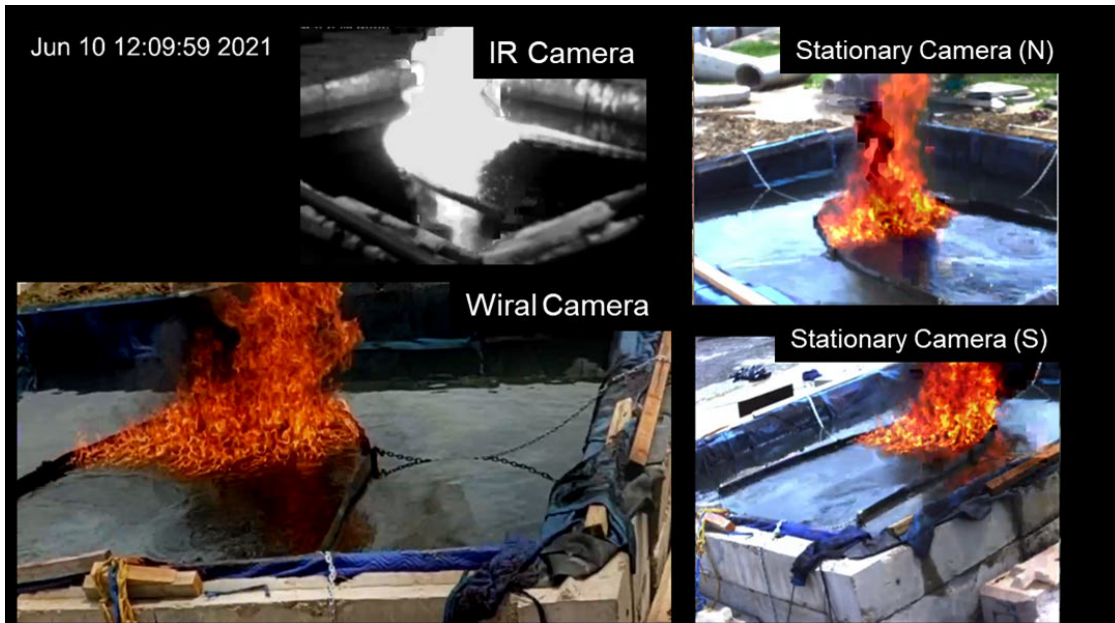# Bureau of Safety and Environmental Enforcement Oil Spill Preparedness Division
Advancement of Quantitative Measurements of ISB Volumes and Burn Rates in Open Water

Final Report

October 2021

(Photo Credit: ARA, 2021)

Paul D. Panetta, Richard Byrne, Alexandria Podolski, and Kevin Panetta

US Department of the Interior
Bureau of Safety and Environmental Enforcement
Oil Spill Preparedness Division

Advancement of Quantitative Measurements of ISB Volumes and Burn Rates in Open Water

Final Report

OSRR # 1108

December 2021

Authors:
Paul Panetta
Applied Research Associates

Richard Byrne

Prepared under 140E0120C0001
By
Applied Research Associates

BSEE

Bureau of Safety and
Environmental
Enforcement

DISCLAIMER

Study concept, oversight, and funding were provided by the US Department of the Interior (DOI), Bureau of Safety and Environmental Enforcement (BSEE), Oil Spill Preparedness Division (OSPD), Sterling, VA, under Contract Number **140E0120C0001**. This report has been technically reviewed by BSEE, and it has been approved for publication. The views and conclusions contained in this document are those of the authors and should not be interpreted as representing the opinions or policies of the US Government, nor does mention of trade names or commercial products constitute endorsement or recommendation for use.

REPORT AVAILABILITY

The PDF file for this report is available through the following sources. Click on the URL and enter the appropriate search term to locate the PDF:

Document Source	Search Term	URL
Bureau of Safety and Environmental Enforcement (BSEE)	Project Number – 1108	https://www.bsee.gov/what-we-do/research/oil-spill-preparedness/oil-spill-response-research
U.S. Department of the Interior Library	Advancement of Quantitative Measurements of ISB Volumes and Burn Rates in Open Water	https://library.doi.gov/uhtbin/cgisirsi/?ps=8L0mpW5uPV/SIRSI/X/60/495/X https://ntrl.ntis.gov/NTRL/
National Technical Reports Library		

Sources: a) BSEE (2019), b) DOI [2021], c) National Technical Information Service (2021)

CITATION

Panetta PD, Byrne R, Podolski A, Panetta K. 2021. Advancement of quantitative measurements of ISB volumes and burn rates in open water. U.S. Department of the Interior, Bureau of Safety and Environmental Enforcement. Report No.: 1108. Contract No.: 140E0120C0001

ABOUT THE COVER

Cover image by Applied Research Associates (ARA) illustrating surface area measurements of burning oil for advancement of in situ burn quantification technology developed under this research effort over previous manual estimations.

Final Report

Advancement of Quantitative Measurements of ISB Volumes and Burn Rates in Open Water

Paul D. Panetta, Ph.D., Richard Byrne, Alexandria Podolski, and Kevin Panetta

Report for

U.S. Department of the Interior

Bureau of Safety and Environmental Enforcement (BSEE)

Sterling, VA

Submitted: October 29, 2021

Updated: December 7, 2021

Acknowledgments

Disclaimer

Table of Contents

List of Figures

List of Tables

1. Executive Summary

This project made significant advancements to the ability to directly measure the volume of oil in the environment and specifically during In-Stu Burning (ISB). The technology advanced into TRL 7 for some aspects and TRL 8 for reproducibility of data. Creating the ability to directly measure the volume of burning oil in a semi-contained burn is a significant accomplishment for the BSEE and the spill response community. This team is the first to create the capability for accurate, real time physical measurements of the volume during semi-contained ISB. We are also the first team to measure the speed of sound of emulsified oils up to 200°C. Advances were made in both the algorithm automation and the hardware integration. In addition to the advancements in technology we performed 65 burns with multiple replicates and quantified the burn rates and efficiencies in multiple ways for HOOPS, Alpine, and Rock for fresh and emulsified oils. The data show that one cannot simply assume a uniform burn rate for these oils since that approach overestimates the burn rate of the various oils. These results advance the technology to enable BSEE and the spill response community to directly measure the volume of oil in the water and the instantaneous burn rates.

Integrating the area and thickness measurements into a single system and deploying it for large scale burns and in the open water will realize this capability for BSEE and the spill response community. The next steps include large scale burns were the oil is free to float or be semi-contained so that boil over can be avoided or studied if needed. The oil control and containment methods will enable direct comparison between burn rates and efficiencies over large range of length scales. Integrating the results of the thickness and area with ERMA is a natural next step that can occur as well.

2. Overview and Objective

In-situ burning (ISB) is an important oil spill response tool for efficient removing oil from the marine environment. For an accurate oil budget calculation, it is critical to quantify the volume of oil removed during ISB. In addition, an accurate measure of the volume of oil removed is important for oil spill responders to gauge the effectiveness of their efforts. The volume of oil consumed during ISB is currently estimated, by manually recording the area of the burning oil using a nomogram, and empirically determined burn rates for that class of oil. While well codified, this method relies on visual estimates of the area, empirical values of burn rate, and does not include a measurement of the thickness. The subjective nature of that method produces inaccurate estimates of the portion of the oil removed by ISB, creating ambiguity in assessing environmental damage, administering fines, and crediting responders for oil removed. The manual process takes attention and time of the person tabulating and recording the information, which could be better used elsewhere during a response action. Complicating this manual process, ISB is a dynamic process. The burning oil does not always fill the boomed area uniformly and the burn rate depends on many factors including type of oil, degree of weathering, thickness, weather conditions, and size of the burn area. An accurate, unbiased measure of the amount of oil removed is an important parameter for oil spill responders, regulators, those monitoring the environmental impact of the spill, and the organization responsible for spilling the oil.

In the previous phase of this work, we developed the basic measurement science to measure the volume of oil from surface area measurements made using aerial camera footage, and slick thickness measurements utilizing using underwater acoustic sensors [1,2,3]. For this phase of work, our objectives were to use the technology we developed to measure the burn rate and efficiency of fresh and emulsified oils on the small scale and fresh oils on the meso-scale, as well as advance the automation of calculating the volume of oil in a slick before, during, and after burning from aerial cameras and underwater acoustic sensors. All these objectives were achieved with the most notable accomplishment being the calculation of the volume of oil on the meso-scale with 1 second temporal resolution, to allow direct knowledge of the instantaneous burn rate and efficiency. The meso-scale slicks were dynamically moving and changing shape and thickness allowing a realistic simulation of an open water environment.

3. TRL advancements of volume measurements during this phase

During this phase, several advancements were made to this technology. Burn rates and efficiencies of ISB of emulsified oils were measured. The fidelity and automation of the software and hardware of the technology were increased, which included integration of the acoustic system with an ROV platform. The reproducibility of the measurement was also advanced through replicate measurements on 3 oils in 5 unique states. These oils ranged from fresh to 20% emulsification with three replicates each, totaling 45 burns. The ISB on the 20 meso-scale burns offered a spill environment that was more closely related to a real spill, with a dynamically changing thickness and surface area of the slick.

3.1. Aerial imaging and surface area algorithm development

The process to extract the area from aerial imagery was primarily focused on using moving imagery from fewer cameras. The Wiral based camera was meant to simulate a camera mounted on a UAV. The refined method transforms the burning area into the bird's eye view

reference frame with a slightly modified methodology from the previous study where fixed cameras were used.

The latest method relies on several specific tracked regions around the fire, such as symbols or markers on the boom, floats, boats, and in the meso-scale test case, the sides of the burn container. The chosen regions were in close proximity in sequential images due to high frame rate, so identifying these markers was quick. Once identified, the changes in the coordinates of the markers between frames are tracked and used to rectify the image to be in the same reference plane and to have the same orientation as the previous image.

Outlines of these aligned images were overlayed to calculate a more accurate surface area. Fire region identification relies on differencing and averaging these overlayed images in order to remove smoke, wind-blown fire obscuring the oil perimeter intersecting the water, and temporary voids in the fire. This alignment method was used so that multiple, consecutive frames could be combined. After processing, the porous fire became smooth, contrasting more with the background which allowed a simple threshold algorithm to detect the perimeter. As an example, a before and after image from the meso-scale burn is shown in Figure 1. This methodology for determining area prepares us for future integration and automated operation.
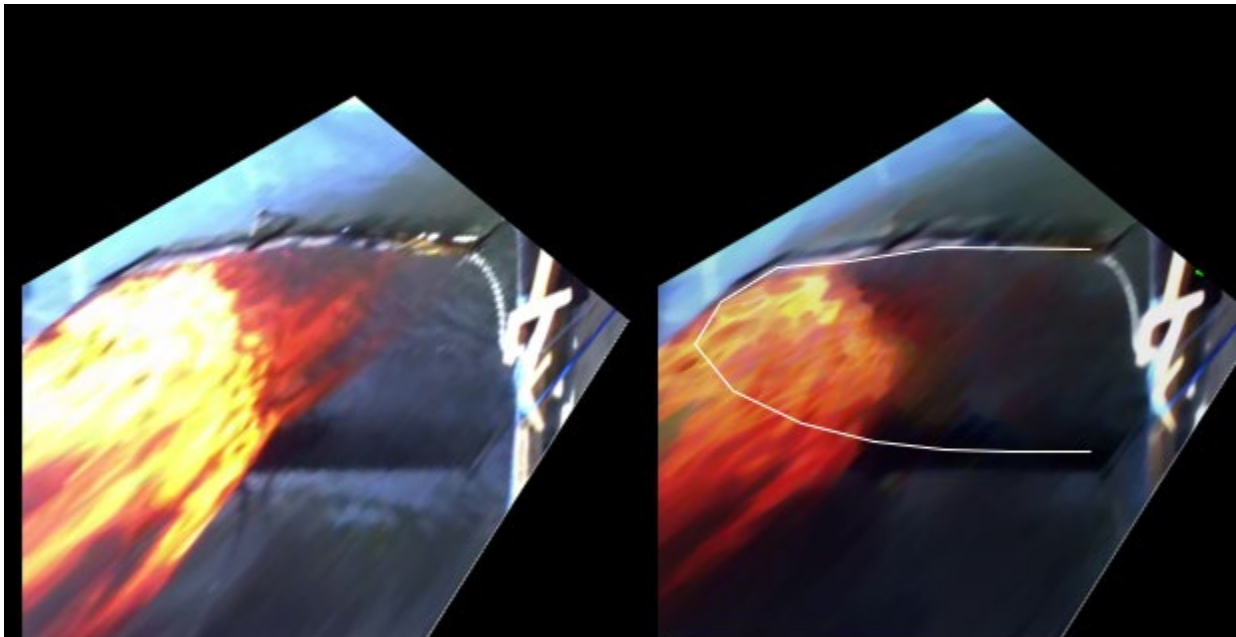
Figure 1: Before (left) and after (right) multi frame processing to see through smoke, wind-blown transient flames.

3.1.1. Initialization

Initial aerial imagery was collected before and after burning began. The imagery was transferred to a computer and the operator ensured the cameras captured clear images of the front perimeter of the fire from multiple angles. The algorithm was then applied to this video stream to identify key regions used to align successive images. The process is set up to be applicable in real time. The initial implementation identified many transient regions, such as water, fire and smoke and static regions such as the boom and boats and other fixed objects. The area calculation is currently semi-automated with the goal to automatically remove the transient

objects and keep the fixed objects in future versions. Though these regions are not entirely static and may drift, the relative change in coordinates in successive images are negligible relative to the transient objects. The tilt angle of the camera is important, as it is used to construct the initial transform. During the work in the first two Phases of this work we found it is best for the camera to be positioned 30 to 45 degrees from the surface of the fire, unless smoke obscured visibility. A low angle camera (<30 degrees) was necessary at times to maintain front perimeter visibility below the smoke.

Camera altitude (a) is also an important parameter that we explored in these first two Phases of work. It is dependent on the camera distance from the fire permiter and the camera angle, as shown in Figure 2. We found for best operation that the camera distance (d) should be dependent both on the field of view and the distance from the fire to ensure the camera is not affected by the heat of the fire. We found the camera angle (θ) needs to be adjusted due to smoke, but will likely be between 30 to 40 degrees from the surface of the flames. The graph on the right in Figure 2 shows the relationship between the Wiral angle (θ) and the Wiral mounted camera altitude (a) for the mesoscale burn with the approximate distance from the fire being 8 feet, calculated using the following equation:

$$d * \tan\theta = a$$

The camera can decrease altitude, and thereby the camera angle, to get under the smoke. The area computation uses the water/fire contrast to calculate area. If the contrast drops along with the computed area, it indicates smoke is obscuring the view enough to merit a lower altitude. The intrinsic camera parameters and the altitude and camera angle will ultimately determine the scale factor. Alternatively, if an object of known length, such as a boom, is in the picture it can be used to determine the scaling of length to number of pixels.
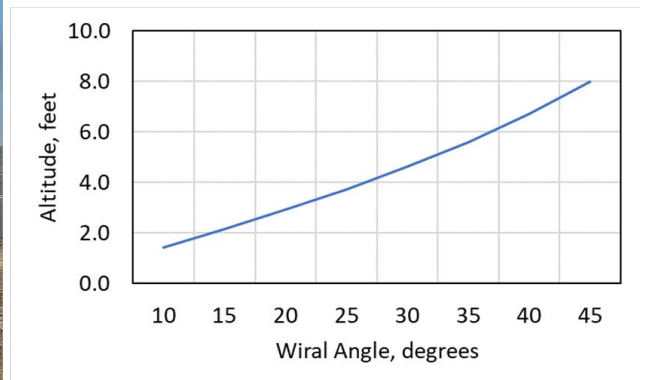
Figure 2 Camera altitude can be calculated with the known camera distance from the fire permiter and camera angle.

3.1.2. Adaptation for missing frames

An important aspect of video surveillance of a dynamic event like ISB is that some frames from the video will not be usable due to a poor field of view due to a poor camera angle or obscuring

from smoke, flames, or other objects. If an image skips between frames, the result might cause a transition point to not match. In this case several frames were discarded until the transition point matches again. As a start, we found 0.5 second worth of frames was a good limit depending of the frames per second for the chosen cameras. If there was still no match, the initialization was re-instated. A camera focused on a point, whether automated or manually operated, will very likely find the point again after a disruption, so re-initialization should be rare. If it does need to happen, there will be a short skip in the area computation interval dependent on the frame rate and length of obscuring.

3.1.3. Pixel counting for area measurements

If a boom is used, the original shape of the boom can be used as a fiducial marker. While the camera was focused primarily on the front perimeter of the fire during the meso-scale burns, the back shape was filled in using the initial boom shape, allowing pixels to be counted on the dynamic portion of the oil/fire. If a free-floating slick is being burned, imagery will need to be collected around the circumference of the fire at a rate that is commensurate with the rate that area is needed. In the case of a free floating slick, the image averaging will consist of a large fraction of the perimeter per computation. The rectified images will be superimposed, and the area will be counted when a new image is generated. Each image placed in the queue and the most recent will contribute most to the outline.

While we found that a boom contained fire only needs a single camera to focus on the front perimeter of the fire, an open fire would require at least two or more cameras for adequate coverage. Additional cameras can easily be added, as the imagery from all cameras will be rectified to contribute to the same perimeter model, as shown in Figure 3.
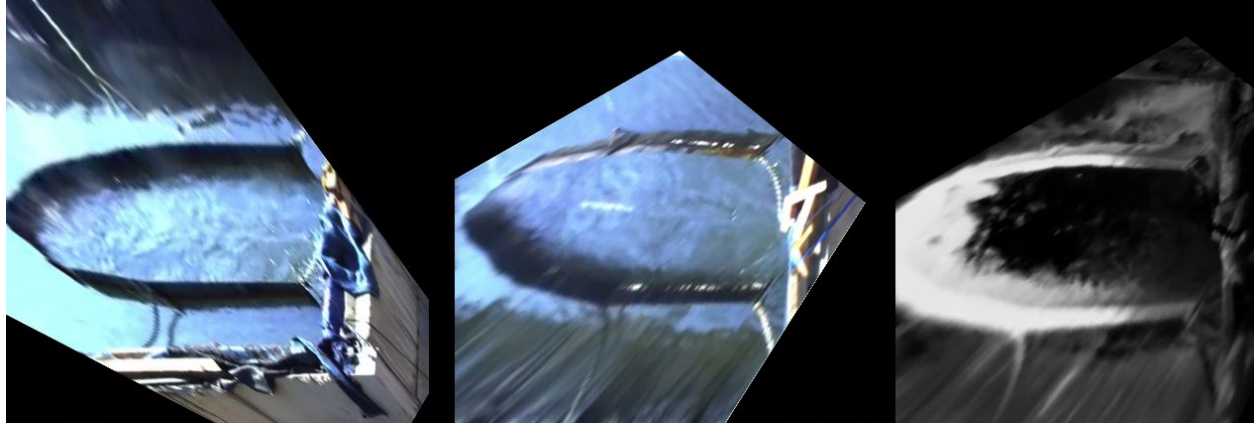
Figure 3: Images from 3 cameras (Meso-scale burn) rectified to the same reference frame can be combined into the same fire perimeter model.

3.1.4. Test Cases

3.1.4.1. UAV video from Canadian Multi-Partner Research Initiative (MPRI) meso-scale burns

Early versions of the algorithms were generated and tested using images from ISB in a large water tank from a Canadian Multi-Partner Research Initiative (MPRI) project where a UAV was used to capture videos of the burning slick. Some of these algorithms were then applied to videos from meso-scale burns to determine burn surface area. Unlike open water burns, the MPRI burns lacked a plane of water surrounding the fire. In this case, the tank rim was slightly elevated from the surface of the water which caused issues with selecting reference points to perform homography, as these points need to be on the same plane. The videos do highlight the circling camera case and have been used to develop the extraction of the full perimeter of the fire as both boomed and free (herded) fires were filmed from the UAV platform. The videos from these two sets of meso-scale burns allowed initial integration and testing of the area calculation from moving cameras. They also allowed identification of technical paths to develop a real time measurement of area on large scale burns and eventually open water burns.
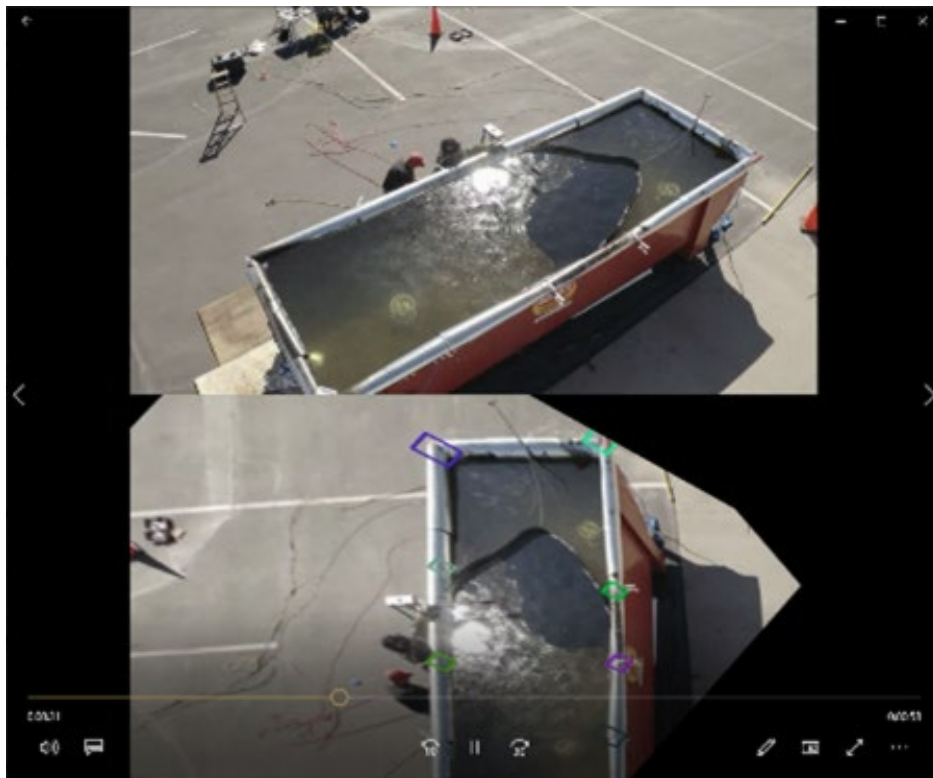
Figure 4: Meso-scale burn with imagery taken from circling UAV (top) and rectified image on bottom. Regions used to align imagery shown as green overlays on bottom image.

3.1.4.2. Meso-scale video

The video taken from the meso-scale burn was streamed through Open Broadcaster Software (OBS). The OBS allows multiple streams to be combined in one display that can be recorded and simultaneously broadcast to the internet. The area calculation code is equipped to extract each frame separately, process the image, and then combine the result.

Figure 5: The meso-scale saved video, which looks exactly like the computer display and is configurable.

3.2. Thickness

During the first phase of this work we focused on the development of the measurement of the thickness of burning oil from static sensors and oil contained in a small area. The measurement of the thickness of oil using acoustic sensors under water from static and ROV platforms has been proven by the team in numerous environments and sea states [4,5]. During this phase we focused on extending those measurement capabilities to small-scale ISB of emulsified oils and meso-scale ISB of dynamically moving oil.

Measuring the thickness of an oil slick using acoustic energy is based on measuring the time that the acoustic wave travels between the bottom of the slick and the top of the slick. Figure 6 illustrates this process and shows reflections from the bottom and top of an oil slick floating on water. To calculate the thickness, one only needs to know the speed of sound of the oil at the temperature the measurement is being made. A detailed discussion of this process is in

numerous reports and publications [1,2,3]. For emulsions we developed methods to measure the speed of sound over the needed temperature range as will be described in a subsequent section.

$$Thickness = \Delta t \, V(T)$$

$V(T)$ = Speed of sound
$\Delta t = time$
T = temperature
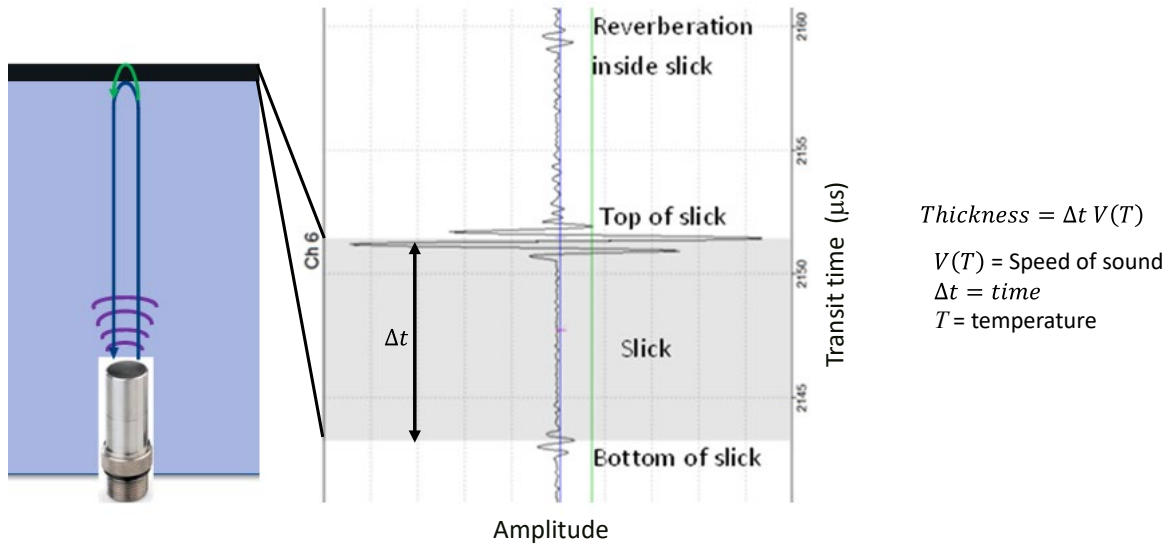
Figure 6. Principle of acoustic slick thickness measurement.

Both the emulsions and the dynamically moving oil offered challenges that needed creative solutions to measure the thickness during burning. We also automated the calculation of the thickness of the fresh and emulsified oils for the small-scale and meso-scale using the harmonic mean approach developed in the previous phase of this work. This automation process was significant since it encompassed 15 states of oil on the small scale and dynamically changing slicks on the meso-scale. Namely the speed of sound of emulsified oils was not known at the temperatures needed. While the effects of the dynamic motion of the oil on the thickness measurements has been developed by the team for floating oil rom ROV platforms in numerous sea states it has not been attempted on burning oil until this phase of work.

An example of the "sonar" image for fresh Rock and an emulsion of Rock with 20% synthetic salt water are shown in Figure 7. The general behavior and features of the sonar images are similar to previous data, however, there are some distinct and important features. Boil-over, a phenomenon seen in in-situ burning, occurs when the water below the slick boils, ejecting water and oil into the air. The sonar image from the fresh oil showed a region with steady burning until approximately 250 seconds when boil-over occurred.   The water moving through the slick can be seen between 250 and ~350 seconds in the region between the bottom and top of the slick.
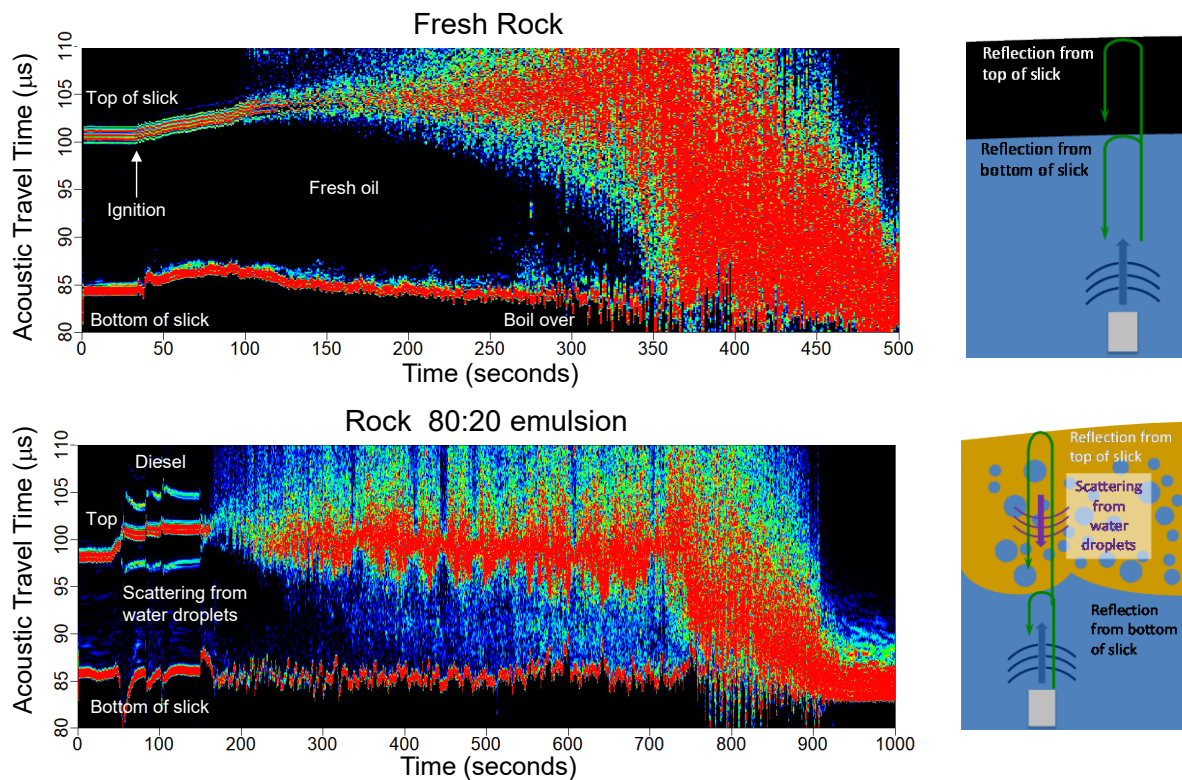
Figure 7. Sonar images from ISB of fresh Rock and an emulsion with 20% water.

The acoustic image from the emulsion was much more dynamic and interesting. The presence of the water droplets in the emulsions was evident immediately due to the significant scattering throughout the slick and indications of the water in the slick increased throughout the burning as more and more water droplets boiled and evaporated as can be seen by the scattering inside the slick starting immediately and increasing through ~750 seconds. For this burn diesel was added as an accelerant prior to igniting the slick. The additions of diesel added prior to burning is evident between 50 and 150 seconds. The 3 distinct additions of diesel can be seen in the data starting at ~50 seconds and extending to ~160 seconds. Once ignited the emulsion behaved similarly to past burns of emulsified oil where the top and bottom surface fluctuated up and down. This behavior is likely due to the agitation of the slick as the water inside the slick boiled and evaporated. Evidence of the water moving through the slick is most clearly seen after ~300 seconds where the scattering from the water droplets inside the slick increases dramatically. Qualitatively these measurements on emulsified oils show the proof of concept to determine if an emulsion is present before and during burning. Further data will be needed to determine the water content and droplet size distribution from the acoustic measurements. Our laboratory measurements confirm these qualitative data as will be discussed in a subsequent section. As far as we know we are the first team to be able to identify the presence of an emulsion of crude oil and water with acoustic measurements. To measure the thickness of these dynamic and unique characteristics of emulsions required advancing the data analysis algorithm to account for the movement of the slick while the water was evaporating from the emulsion and to accurately identify the bottom and top of the slick.

3.2.1. Universal speed of sound

In the open water during a spill response, the temperature inside the burning slick will likley not be known or measurable. To determine the thickness when no temperature information is available requires a speed of sound for burning oil as a function of time. The approach used for the small scale burns identified a speed of sound as a function of time for each oil during the burn. Those speeds of sound identified form the basis for a universal speed of sound as a function of time for application to other burns of the same oil and same size. On the small scale, the burning times of each oil were very similar allowing that universal speed of sound as a function of time to be used on contained burns.

The meso-scale burns were more dynamic and the universal speed of sound as a function of time applied from the small scale burns did not accurately represent the thickness for those burns. For the small scale burns, once the surface of the oil was covered with flames, which happened almost instantly, the thickness began to decrease due to the fact that the oil as confined. For the mesoscale burns both the area and thickness changed continuously during the burn due to the uncontained nature of the oil in the boom and the dynamic use of the ice eaters. That dynamic behavior is more similar to an open water burn and very different from the small contained burns. To effectively develop a universal speed of sound for semi-contained burns and free floating burns will require additional burns with systematic control of the thickness and area during the burn as well as the total burn time.

3.2.2. Acoustic sensor deployment

Optimum deployment of the acoustic sensors depends on the spill environment. For fixed tanks or small scale burns, the acoustic sensors were deployed on a fixed frame placed on the bottom of the tank or on a fixed frame. For other environments including deeper tanks or open water the sensors were deployed on various ROV platforms in various sea states [3,4,5]. Typically, the sensors were placed anywhere from 1 cm below the water surface to over 7 feet deep. The depth of the sensor has not affected accuracy or precision of the data, but should be explored for open water environments as the ROV may need to be deeper than 7 feet below the surface. However, many current ROVs have a depth hold feature that allows controlled operation at shallow depths (<7 feet) that we have used for slick thickness measurements. Also, for slick thickness measurements in waves the sensors need to be installed to accommodate the pitch and roll of the ROV and relative movement of the water surface. We deployed the sensors on several ROVs and successfully measured the slick thickness in waves as high as 22 inches from peak to trough [5].

3.3. Volume

During the first phase of this work and in the previous small-scale burns the oil typically covered the entire surface of the water, thus development of surface area and volume measurements were not advanced. During this phase of work the for the meso-scale burns the oil was partially contained in simulated boom and the surface area was dynamically changing allowing for advancement of the surface area, thickness, and thus volume measurements. An example of the partially contained oil is shown in Figure 8.

Figure 8. ISB of 19 Liters (5 gallons) of HOOPS in a simulated boom.

3.4. Aerial Cameras

Monitoring an ISB at sea may be one of the most dynamic scenes possible. The fire and water are constantly in motion, changing frame to frame. During this project, we developed novel aerial imagery collection methods for research-scale in-situ burns to aid in the development of algorithms to ultimately compute a live accurate burn area from a moving aerial camera. These methods were refined throughout the course of four different period's of in-situ burns. Ideally unmanned aerial vehicles (UAV) carrying cameras would be used. However, UAVs were not allowed on this project this we were required utilize an alternative method to move the cameras in the air to simulate UAV operation.

3.5. Wiral Functionality

Wiral Lite cable camera systems were used to accommodate the elimination of UAVs during all in-situ burns performed for this project. Wirals are a remote-controlled system to hold a camera on a suspended cord to allow movement along a line. Each Wiral has a hand-held controller to move the camera with various modalities. The ping pong modality, where the camera moved at a set speed back and forth between two set points, was used to mimic the movement of a UAV during the in-situ burns. A Wiral system is shown in Figure 9.

Wiral Lite Cable Cam with GoPro

Figure 9: Wiral Cable Cam and GoPro.

Early on, three limitations were identified:

1. All active Wiral units could only respond to a single remote, forcing all Wirals to adhere to the same pattern.

2. Wiral remotes had a limited communication distance, likely due to the distance between the units and the low power of the remote.

3. The left and right stop drifted over time when using ping pong mode, likely due to an angle in the Wiral cable.

To address the current known limitations of the Wiral hand-held controllers, work was done to examine various methods to boost the range of the Wiral controllers and make each one independently controllable through a computer interface. The ability for the Wirals controls to be 'digitized' and controlled by a computer was imperative in the event of large-scale burns. The easiest way to implement the computer control and range extension was to connect wires from the controller to a radio and incorporate the controller circuit board into the body of the Wiral. We embarked on this approach and connected the relay for each control to a radio output port so instructions across the radio bridge could simulate each button. The feedback from the Wiral could then be read off voltages from the indicator lights and sent back. All these signals could be transmitted to an Xbee radio that was digitally connected to the computer. The integrated concept is shown in Figure 10 and will fix the unexpected short range issues and allow for computer control for seamless integration with the data collection especially for large-scale burns.

Current Wiral set up

Controller circuit

Phone Cam.

Battery pack

Hand-held controller

Improved Wiral set up

Controller circuit

Xbee radio

Phone Cam.

Battery pack

Computer controlled
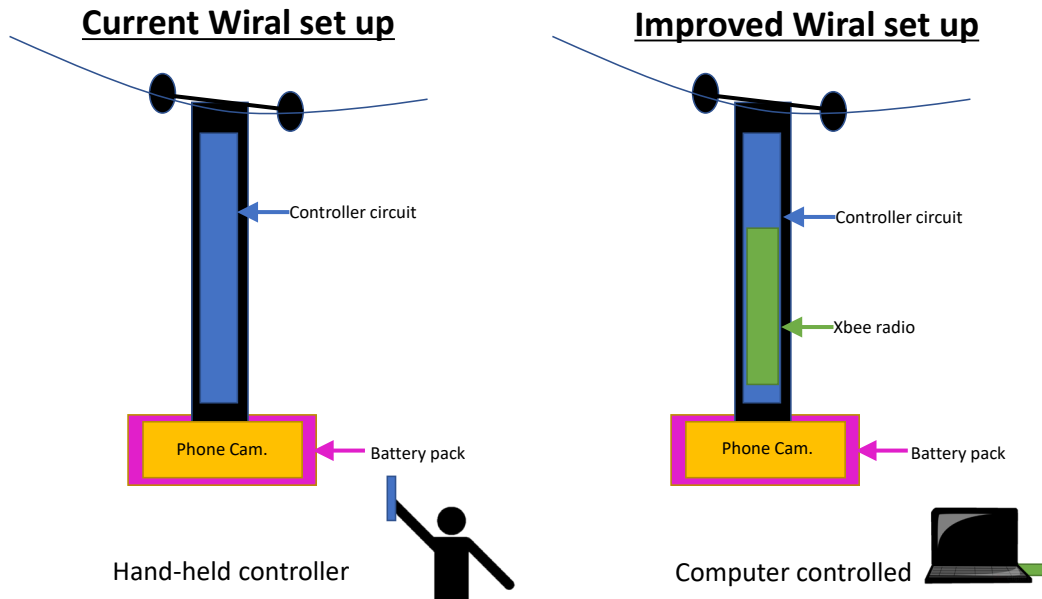
Figure 10. Schematic of computer controlled Wiral deployment.

3.6. Aerial Camera Iteration

Cameras mounted to the Wiral Lite cable systems were iterated upon to address evolving needs throughout the project. In the initial small-scale burns of HOOPS in October 2020, a GoPro was mounted to the Wiral at an approximate 45° angle to the burn. While GoPros are useful for capturing video for various scenarios, streaming the live videos to a hard drive is beyond their design capabilities. Because of this limitation, coordinating ROV movement, acoustic measurements, and camera images and videos became near-impossible while using the GoPros.

To implement a low-risk, high quality solution, we systematically assessed the risks (technical, schedule, and budget) of several camera systems. We also assessed the overall quality of solution which incorporated the ease of use, robustness, and design of the camera systems to directly stream to a computer hard drive. The assessment is shown in Table 1 with a lower score indicating a lower risk and better solution. The GoPro was rated very poorly due mostly to the cumbersome nature for connecting to the computer.

Table 1. Risk assessment for camera options.

Device	Technical Risk	Schedule Risk	Budget Risk	Quality of Solution	Risk Only	Overall Score
Smart Phone	1	3	3	2	7	9
Security Camera	3	3	2	1	8	9
UAV	3	3	4	1	10	11
GoPro	3	3	1	5	7	12
Raspberry Pi	4	3	3	3	10	13

The risk assessment identified two viable solutions that could allow for streaming live videos to a hard drive: IP Security cameras and smartphones. IP Security cameras were investigated as a viable option, as they are very inexpensive, can function as basic IP cameras, and have wireless battery powered options. Ultimately, IP Security cameras were deemed a technical risk for this project. Not only is there significant variation between models requiring time and research to understand, but security cameras would have required additional work to override features such as motion detection activation, which far beyond the scope of this project.

Smart phones were selected as the lowest risk, and highest quality solution due to their high resolution, simplicity of use, and streaming reliability seen in the lab. Smart phones were used to collect video footage for small scale burns of Rock and Alpine, as well as all meso-scale burns. During small scale burns of Rock, the smart phones were mounted with battery packs to the Wirals using gear ties and duct tape at an angle 45° to the fire. With a battery pack the phone was able to stay aloft and transit videos real-time and remain 100% charged all day. The initial mounting method was improved upon for the Alpine burns, using Wiral manufactured smartphone attachments. The smart phone mounting method was finally modified to include a pouch for an ice pack for the meso-scale burns, during which the smart phones were prone to overheating during the 100°F summer days. Stationary cameras (infrared and machine vision cameras) supplemented aerial cameras, and could be relied upon to maintain the same angle and distance to the fire and therefore allowed the use of the same transfer function to convert pixels-to-area throughout the burn during algorithm development.

Table 2. Decision matrix to inform our decision to further investigate a subset of camera technology, where low score are more desirable.

Device	Technical Risk	Schedule Risk	Budget Risk	Quality of Solution	Risk Only	Overall Score
GoPro	4	3	1	5	8	13
Smart Phone	1	3	3	4	7	11
Raspberry Pi	3	3	3	4	9	13
Security Camera	5	3	2	1	10	11
UAV	3	3	3	1	9	10

3.7. Aerial footage streaming

To stream the videos to the hard drive synchronously with the temperature, mass, and acoustic measurements, video streams were accessed by a single PC and combined using the Open Broadcaster Software (OBS) studio application. The application provides flexible configuration of the onscreen display of any number of streams from different sources using varied streaming methods and records video to disk. The application is open source and available for free. A screenshot of the resultant system during meso-scale burning is shown in Figure 11. These simultaneous video and data streams were recorded directly onto two separate computers for the project data analysis purposes.
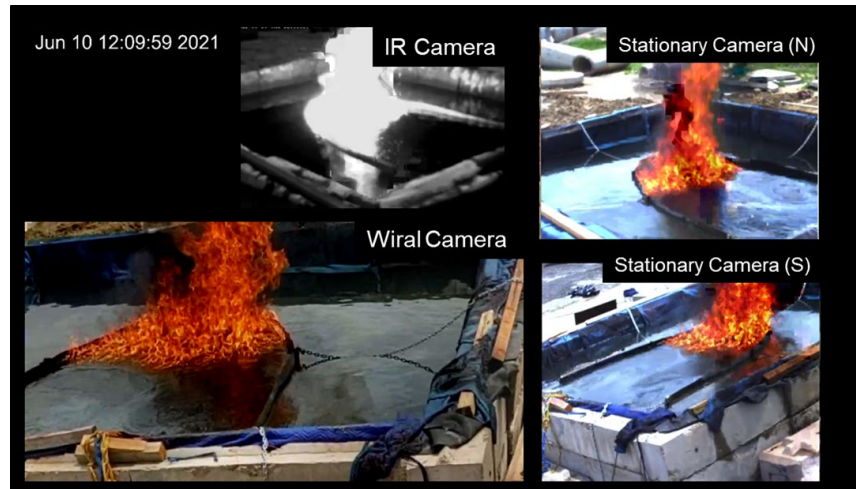
Figure 11. Screenshot of footage collected from 4 cameras during burn 10, a 7.5 gallon burn of HOOPS.

They were also and live-streamed over the cellular phone network around North America to enable people who could not travel to be engaged and be involved on the burns (see Figure 11). There were approximately 50 distinct viewers, with many of them tuning in more than once. It was notable that both BSEE contracting personnel dialed in. We also had representatives from the Canadian MPRI online as well as representatives from Poker Flat, EPA, NOAA, Environment Canada, Natural Resources Canada and many other organizations.   The live streaming was directly valuable for the COR and team members, who could not be onsite due to COVID-19 travel restrictions. They were able to participate and see the action as well as direct cameras and activities throughout the week. The live-stream also made the broader oil spill response community more aware of our work and enabled them to follow our activities.   For some viewers, it was the first time they saw in-situ burning on any scale.
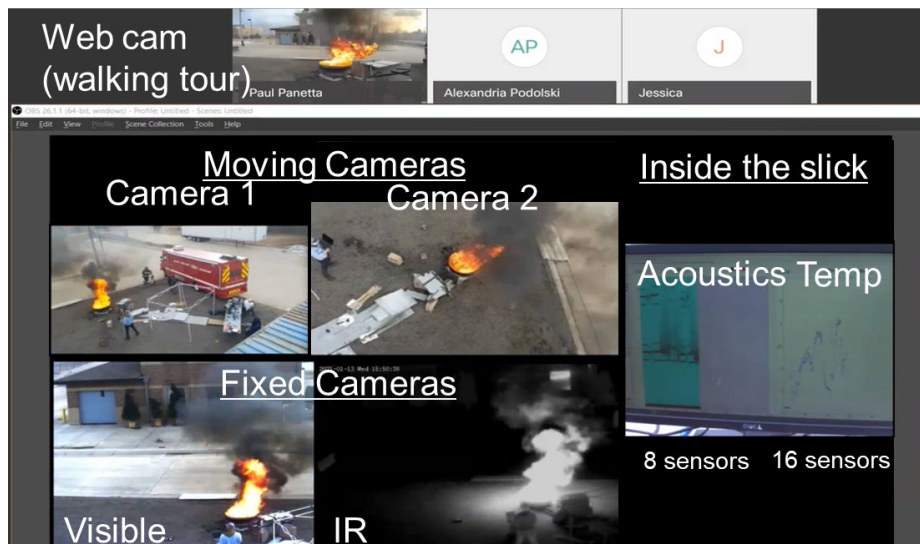
Figure 12 Used OBS to simultaneously view and record video streams from an iDS machine vision camera, an infrared camera, and an aerial cameras.

3.8. ROV compatability

During the development of slick thickness measurements over the last 8 years, the team has used 5 different ROV and two AUV platforms in various sea states [4,5]. There are 3 key aspects needed for implementing slick thickness measurements.

    1. **Physical compatibility of the platform** - the ROV needs to be able to move in a manner that allows the acoustic sensor to remain perpendicular to the surface.

    2. **Electronic compatibility of the platform** - the electronic noise from the ROV system needs to be low enough to allow measurement of the slick thickness.

    3. **Integration capability** – the ROV must be capable of operating using an integrated acoustic system including the onboard power and using the communications tether.

For this project we focused on assessing two observation-class ROVs: the BlueROV2 and the Deep Trekker DTX2. Images of the ROVs with acoustic sensors are shown below.

3.8.1. BlueROV2

The BlueROV2 is a low cost ROV that comes as a kit that needs to be assembled. The software is open source and offers maximum customizability in the hardware and software. The open source nature of the system offers maximum flexibility; however, one must be proficient at ROV operations, assembly, and software debugging. Once operational, it is quite a powerful ROV with great maneuverability and easy operation.

1. Physical compatibility

    a. The BlueROV2 shines in maneuverability and overall physical compatibility for acoustic thickness measurements. The ROV can move in any direction and maintain its orientation, pitch and roll, and depth. These capabilities are ideal for slick thickness measurements because the sensors need to maintain a perpendicular orientation to the surface, ideally a stable depth.

    b. The "do it yourself" nature of the BlueROV2 and low cost of construction materials has led to some reliability issues. We are working with the manufacturer to determine if a manufacturing defect is the culprit or if reassembly is needed.

2. Electronic Compatibility

    a. The electronic system of the BlueROV2 causes a large amount of electronic noise relative to other ROVs. While significant, the electronic noise can be mitigated with appropriate hardware settings on the acoustic system used for this project and software post processing methods.

3. Acoustic integration potential

    a. The BlueROV2 allowed for easy integration of the acoustic system we have been using for the BSEE projects. The connection to the electronics and communication tether was seamless and inexpensive.

Overall assessment: For this stage of development, the BlueROV2 is an ideal platform because of its ease of use and customizability, as well as its traditional and nimble movement and low cost. The robustness of the system is still being reviewed and will be an important aspect going forward.

3.8.2. Deep Trekker DTX2

The Deep Trekker DTX2 ROV is a more expensive system than the BlueROV2. It is well built with simple, easy to use controls that are very reliable. The specifications of this observation class ROV in terms of speed, depths rating, and payload are nearly identical to the BlueROV2 and other ROVs in this class. The assessment is below.

1. Physical compatibility

    a. The Deep Trekker utilizes full-body motion to adjust depth that results in the ROV pitching forward to move down and pitching backward to move up, see Figure 13. This type of motion is unique to Deep Trekker and while it offers instant maneuverability, it is severely limiting for slick thickness measurements because measuring slick thickness requires constant micro-adjustments of ROV depth. This motion is not compatible with slick thickness measurements because the sensors move dramatically away from perpendicular to the surface during movement up and down. This motion would create data loss and the potential to lose the location of the slick in the acoustic field of view entirely.

2. Electronic Compatibility

    a. The electronic system of the Deep Trekker has much lower electronic noise than the BlueROV2 and other ROVs used in the past. The electronic noise is still measurable but can be much more easily mitigated with easy hardware settings on the acoustic system or with no modifications.   This aspect is very desirable and notably good.

3. Acoustic integration potential

    a. The Deep Trekker offers some integration with sonar and acoustic systems, but at higher costs than the BlueROV2. In addition, this particular model has been discontinued and replaced with a similar configuration. The system comes with its own controller and does not offer computer control, thus if the acoustic system could be integrated into the ROV, usage would require two operators and a separate computer to acquire acoustic data.

Moving up

Acoustic sensor tilted back

Moving forward

Acoustic sensor vertical

Moving down

Acoustic sensor tilted forward
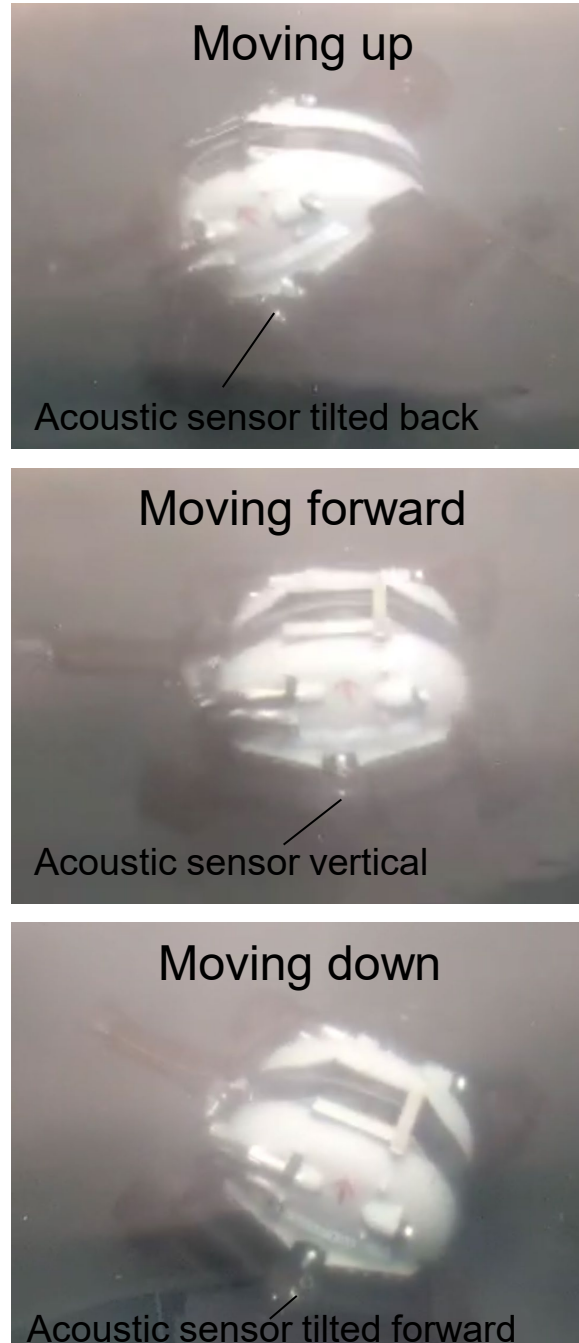
Figure 13. Pitch of Deep Trekker ROV when moving up and down. The acoustic sensor tilts back and forward when the ROV moves up and down in the water column.

Overall assessment:

The Deep Trekker ROV is electronically reliable and robust but is physically incompatible with slick thickness measurements. This incompatibility eliminates the Deep Trekker ROV from further pursuit. There is a large selection of other ROVs that maneuver in the more traditional manner from many ROV companies.

3.9. Integration with ROV and Wiral

The acoustic (sonar) system was integrated into the BleeROV2 platform in terms of communication, electrical power, and physical mounting as shown in Figure 14. The acoustic system was powered by the ROV battery and communication to the computer went through the same tether used to communicate with the ROV. The acoustic system was mounted in a separate enclosure underneath the main ROV body.
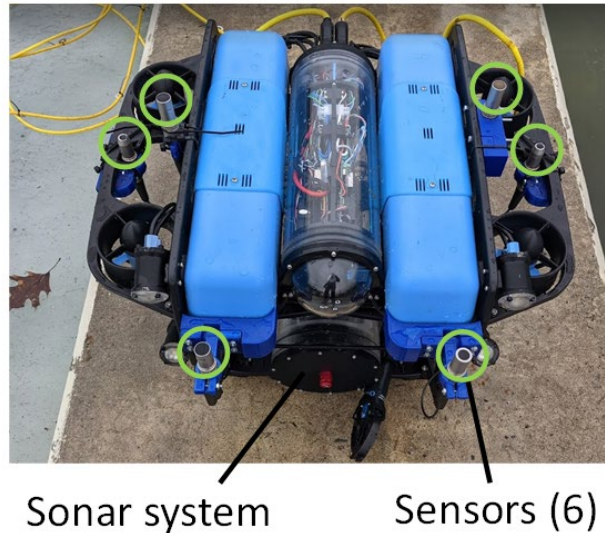
Figure 14. BlueROV2 with integrated acoustic system with acoustic sensors indicated with green circles.

To determine the maneuverability of an ROV and work on the operation of the Wiral in coordination with ROV movement, acoustic data collection, and video collection we tested these systems at a local lake in Colorado. An image of the lake and setup area is shown in Figure 15. The BlueROV2 with three acoustic sensors is shown in Figure 16.
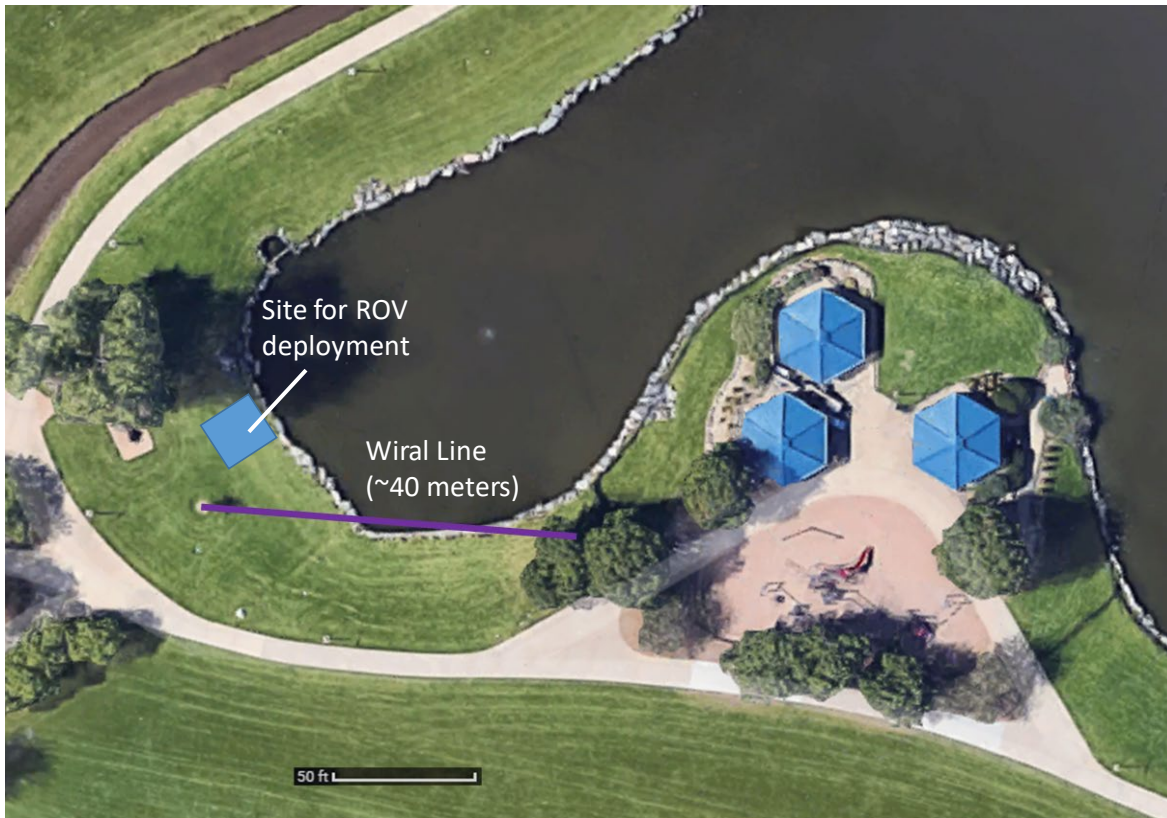
Figure 15: Test site for ROV deployment and Wiral setup.

Figure 16: BlueROV2 with acoustic sensors.

An image of the Wiral and ROV is shown in Figure 17. The ROV was flown independently from the Wiral operation to allow the operator to become familiar with open water operation in a quiescent body of water. The Wiral was operated both manually and in "ping pong" mode. Ping

pong is the official term used by the manufacturer to describe the mode where the Wirals automatically move in one direction until they meet a manually set stop and then reverse automatically and proceed in the other direction to the other stop until directed to stop or battery power is depleted. The set up and operation was simple and allowed imaging of the ROV from many angles. The handheld controller has limited range and the system often stopped when the user was too far from the system.
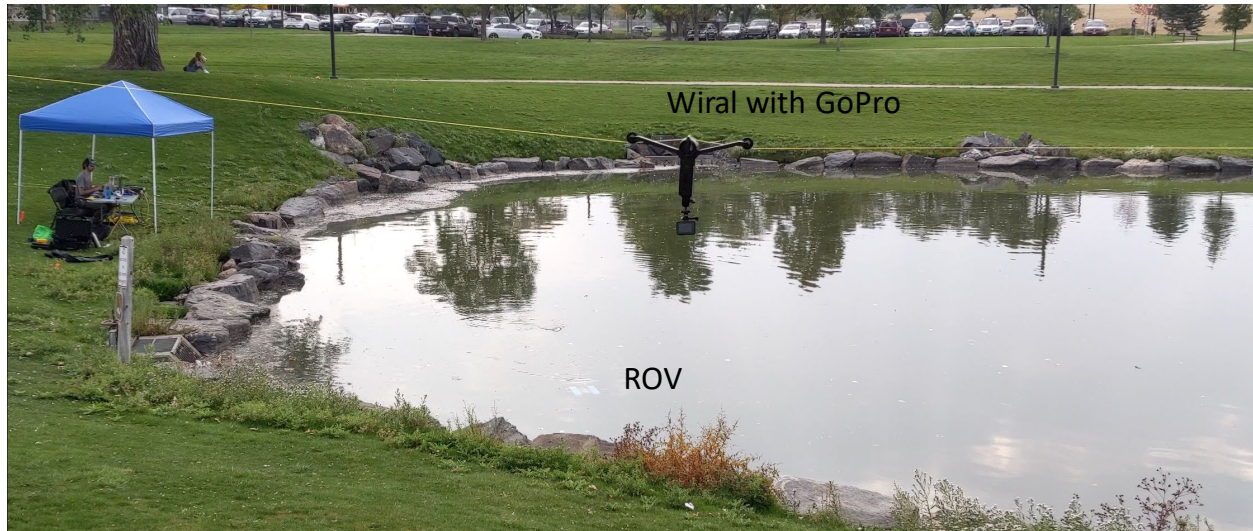
Figure 17: The ROV and Wiral in operation.

Figure 18 shows an image of the ROV in the water from the GoPro on the Wiral as they traversed the test area. The resultant acoustic profile of the bottom of the lake is shown in Figure 19. The ROV and Wiral-GoPro system were simple to use and quite functional for performing simultaneous imaging and ROV operation.

Figure 18: Image of the ROV performing an acoustic profile of the bottom of the lake from the Wiral mounted GoPro
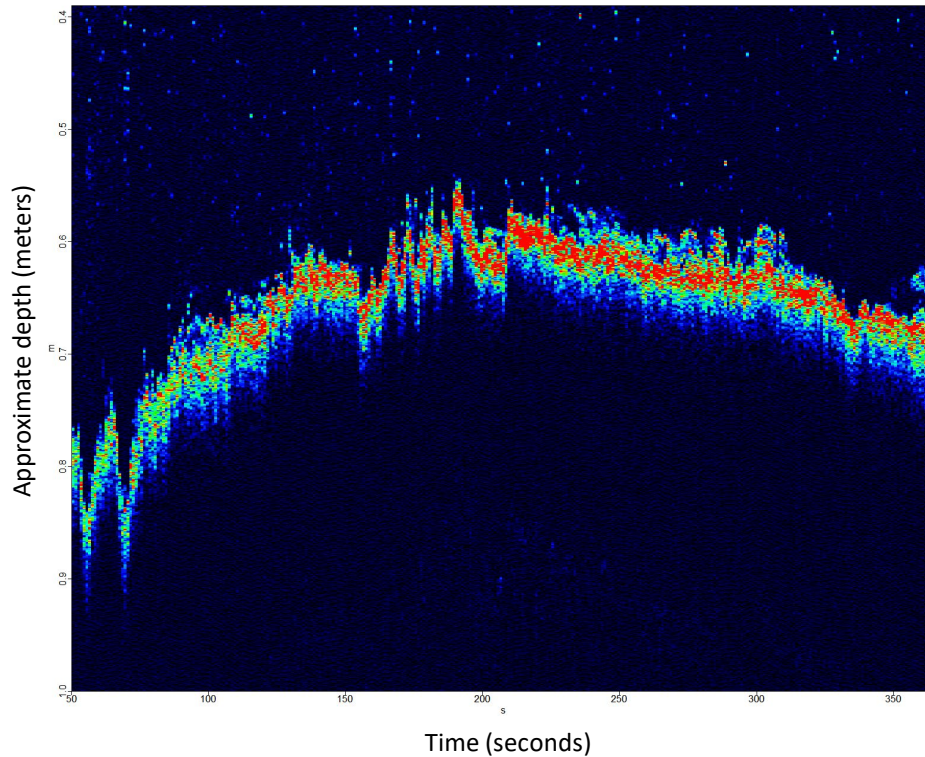
Figure 19: Acoustic profile of the bottom of the lake.

4. Emulsion making and characterization

ISB of emulsified oils were the main focus of research for this phase of work.

4.1. Weathering methods

HOOPS and Alpine weathered in a two-step process involving evaporation and then emulsification. These oils were first exposed to an evaporation process to increase the percentage of asphaltenes, which are known to help stabilize emulsions of water in oil. First, oil was aerated in a 50-gallon drum using an air sparging system. The air compressor's tank pressure was 90psi with a flow rate of 3 cubic feet per minute. The drums were partially covered to reduce spill-over. Once a mass loss of ~15% by weight was achieved, oil was emulsified using a variable speed mixer.
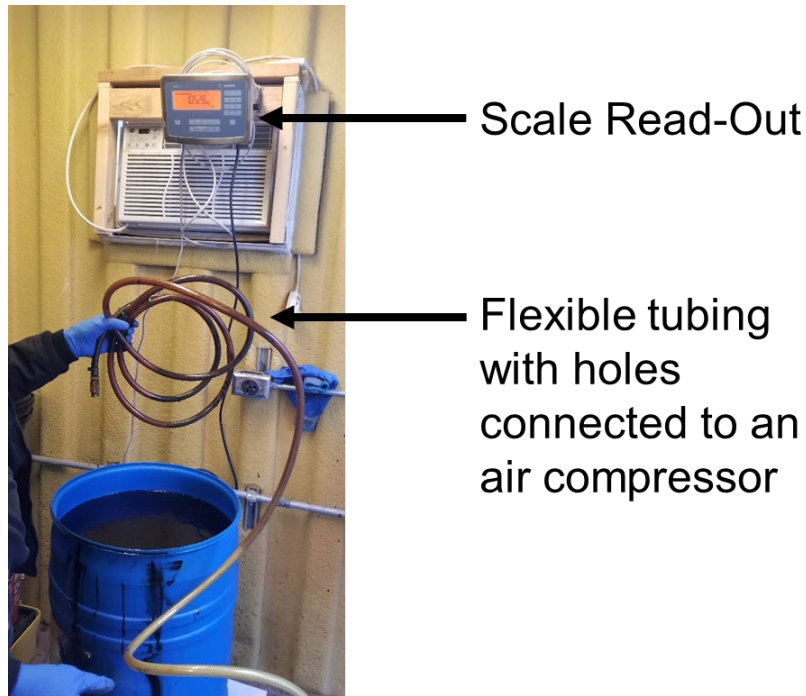
Figure 20 Air sparging system to evaporatively weather oils was comprised of flexible tubing with small holes attached to an air compressor.

4.1.1. Mixing procedure

For the mixing process, we chose to use a 0.5 hp variable speed mixer. As seen in Figure 21, a ¾ inch stainless steel shaft with a concrete mixing blade was used. The heavy concrete mixing blade in conjunction with the ¾ inch stainless shaft, helped eliminate vibration that caused the mixing of unwanted air into the emulsion and out of control vibrations. As seen in Figure 21, multiple baffles were installed in the bucket to help increase in shearing energy and ensure quality mixing. In addition to the baffles, a tap was installed at the bottom of the bucket to check for separation of the emulsion. To further prevent air from being mixed into the emulsion, we tested different shaft speeds. The best shaft speed at preventing air from being mixed in while maintaining a good speed was 200-300 RPM. As seen in Figure 22 the shaft speed was measured with a laser tachometer every hour to keep optimal performance. Emulsions with water content of 5%, 10%, 15% and 20% were made in a 5-gallon bucket and in 50 gallon drums depending on the volumes needed. The mixer was secured to a rigid structure built of 80/20 to reduce impact of vibrations produced by the mixer during operations. Mixing time we typically 30 or more hours for each emulsion depending on the water content and the viscosity of the fresh oil. Generally, higher viscosity oils and lower water content emulsions stabilized more quickly.

Figure 21. Emulsion Mixing Apparatus and Motor Shaft

Figure 22: Digital readout of shaft speed.

4.2. Solutions to uncontrolled vibrations

Several problems with the first iteration of the motor shaft led to uncontrolled vibrations which caused the end of the mixing blade to move over 2 feet when speed was over 150 RPM. The excursion was so extreme that it bent a steel paint mixer, as seen in Figure 23. Our solution was

to use a thicker ¾ inch motor shaft with the mixing blade attached to the thicker shaft. To contain the minor vibrations still present the motor was strapped to the wall (see Figure 23). The resultant set up allowed safe operation through the full range of the mixer speed up to ~1400 RPM.

Figure 23. Motor Shafts & Improved Motor Mount

Table 3. Emulsions of ANS

Batch	Oil	Evaporative Loss	Water Content	Air Sparging Time	Mixing Time
First Emulsion	ANS	13.6%	20%	42 Hours	30 Hours
Second Emulsion	ANS	12.2%	20%	56 Hours	35 Hours

4.2.1. Verification of stable emulsion

A microscope with a digital camera was used to analyze and photograph 1mL samples of the emulsion throughout the mixing process to evaluate if the oil was sufficiently emulsified. As mixing time increased, the water droplets suspended in the oil decreased in size and became increasingly uniform. A stable emulsion is formed when there is no significant change in droplet size between samples despite continuous mixing. Of the three oils that were weathered, Rock was the fastest to emulsify and remained stable the longest when compared to HOOPS and Alpine.

4.3. Microscopy

To confirm that an emulsion was made and the document progression, a microscope seen in Figure 24 was used. 1 mL of the emulsion was applied on a single concave slide and allowed to coat its entirety. As seen in Figure 24 the slide was rotated and held perpendicular to the ground to coat the slide.
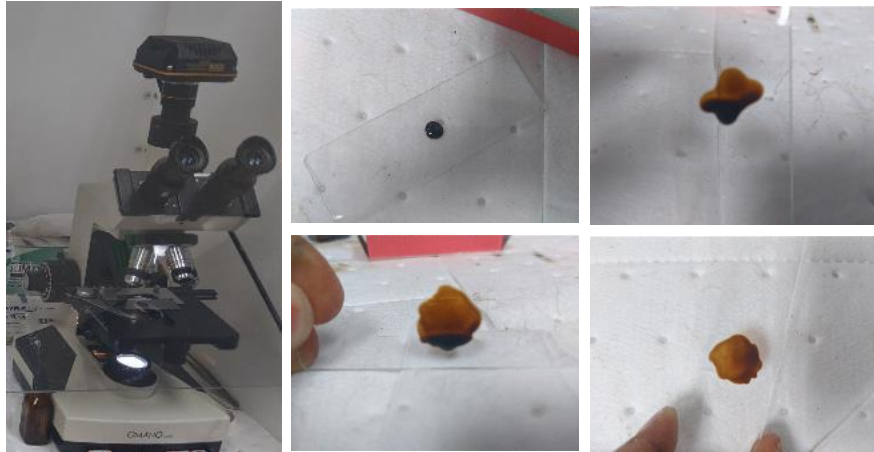
Figure 24. Microscope & Slide prep

We took photos of the emulsion every hour to document any change in the emulsion. As seen in Figure 25 with additional mixing time, the water droplets became increasingly uniform and continued to decrease in size. After ~27 hours, the droplet size stabilized but kept grouping closer together. At the 32-hour mark, there was little to no visible change in the droplets of the emulsion. The droplet morphology maintained this state over the next 10 hours of mixing. Based on the visible stability of the water droplets for this emulsion it is estimated that about 35 hours of mixing was needed to create a stable emulsion. This process was used to verify the stability of all emulsions made for this project.
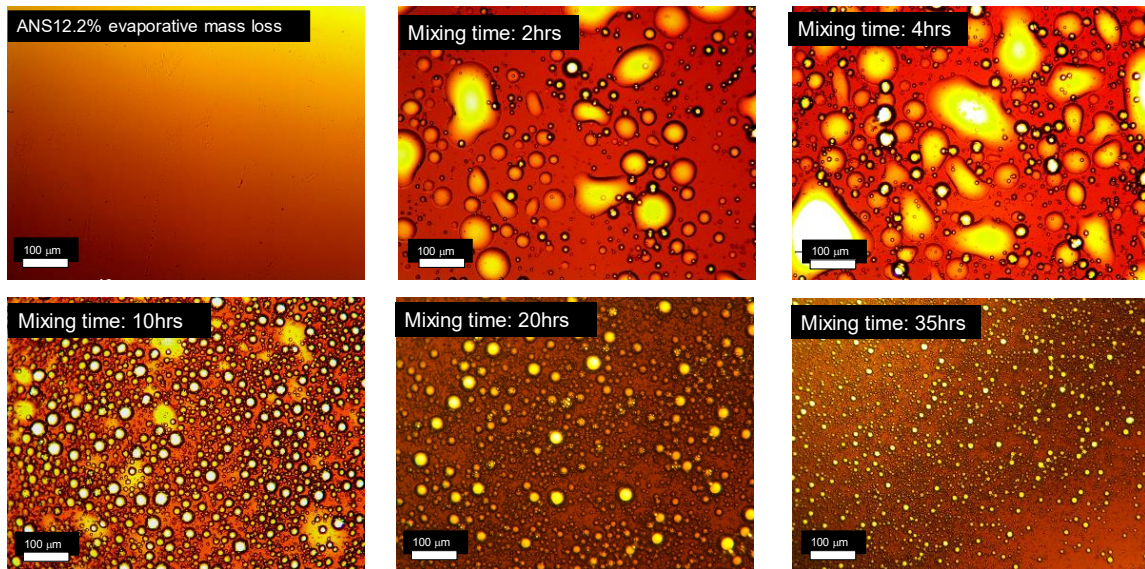
Figure 25. Photos Emulsion Batch 2 (ANS 20% Water 12.2% Evaporative Loss)

4.4. Water content & stability

The water content of the emulsions as well the stability was measured over several weeks. We placed 250 mL of emulsified oil in a separation funnel. The separation of the water from the emulsion was not linear in time; it took about one week for any real change to be seen and two weeks for most of the water to separate. By three weeks, 50mL of water had precipitated out of solution, the oil was left to sit for one more week to ensure complete separation.

24 hours after mixing
(negligible separation)

72 hours (3 days) after mixing
(negligible separation)

4 weeks after mixing
(100% separation)
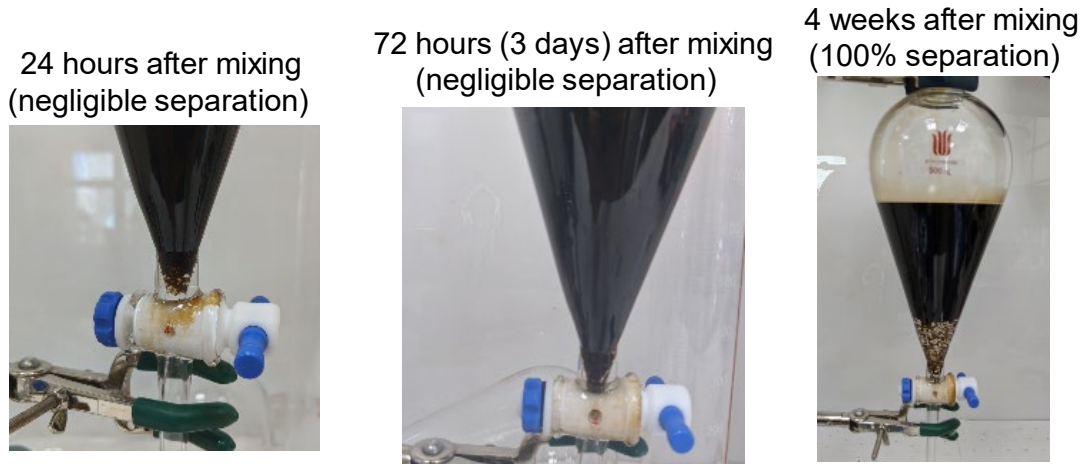
Figure 26. Visual Indication of Stability of Emulsion over 4 weeks

4.5. Speed of sound measurements of fresh and emulsified oils

Prior to the work performed during this project, there were no reported speed of sound measurements for emulsified oils at the temperatures needed for this work. Thus, speed of sound was measured for HOOPS, Rock and Alpine subjected to evaporation and emulsification with a water content of 5%, 10%, 15% and 20%. While some change in methodology from measuring the speed of sound for fresh oils was anticipated, several challenges emerged that resulted in the evolution of speed of sound measurement methods.
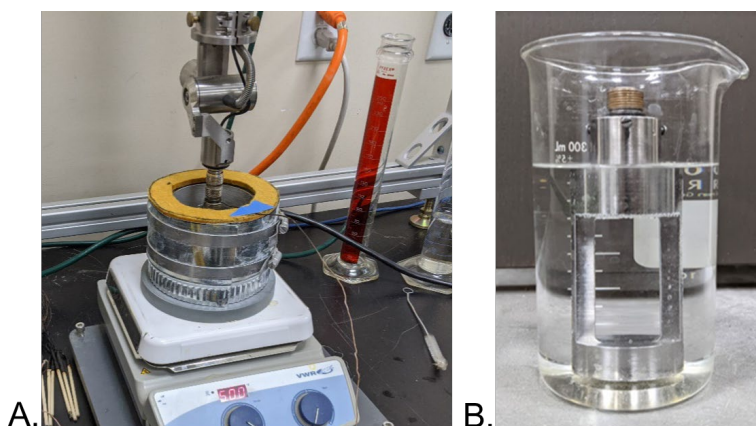
Speed of sound measurements were made using a previously fabricated transducer reflector which allowed for a near-constant distance between the transducer and the reflector plate. The transducer reflector was placed into a container with approximately 250 mL of oil. Using a hot plate, the temperature of oil was steadily increased to temperatures between 20-200ºC during which measurements were taken with 1 second temporal resolution.

Initial measurements were made in a highly insulated container to minimize fluctuation in temperature, however this highly insulated container resulted in spontaneous boil over for lower viscosity oils and emulsions at temperatures exceeding 100ºC. To decrease the risk of boil over, measurement collection time was extended to allow light ends to potentially evaporate off. Additionally, the insulated container was replaced with a Pyrex glass beaker in the hope that temperature changes would be more gradual throughout the volume. Unfortunately, some boil over still occurred. Future mitigation strategies could involve using boiling chips, however, the transducer reflector may need modifications to prevent chips from coming between the transducer and reflection plate, thereby interfering with the speed of sound measurement. See Figure 27 and Figure 28.

Figure 27. Transducer with reflector as drawn (left), as fabricated (right).

A.   B.

Figure 28 Speed of sound measurements were collected in an iterative process, as each new emulsified oil presented new challenges. While speed of sound in fresh oil could be measured in a highly insulated container (A.), speed of sound in most emulsions had to be made in an open top beaker with a transducer reflector (B.).

Using these methods the speed of sound was collected for fresh and emulsified HOOPS, Alpine, and Rock up to 20% water up to 200°C. An example of the speed of sound as a function of temperature for fresh Rock is shown in Figure 29 for 3 replicates. The curve fit to run 3 is also shown along. These data are typical in terms of reproducibility and quality of the fit with the R^2 value very close to 1. The curve fitting values are shown in Table 4 and the resultant speed of sound as a function of temperature for the thickness measurements during ISB are shown in Figure 30.

Rock Fresh Speed of Sound

$y = 1.567E+00e^{-2.397E-03x}$
$R^2 = 9.954E-01$
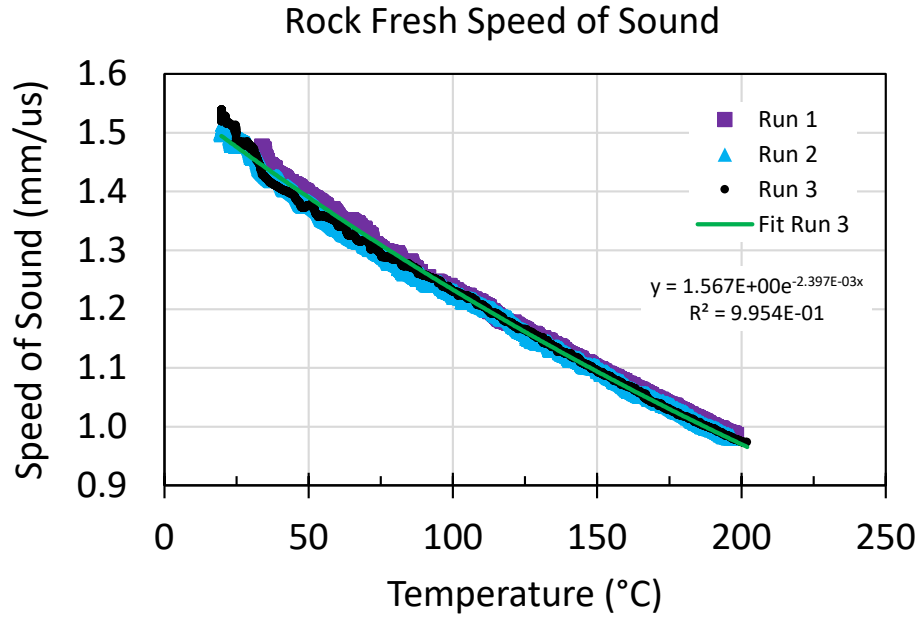
Figure 29. Speed of sound from 3 replicate runs for fresh Rock up to 200°C.

Table 4. Speed of sound as a function of temperature for the 15 states of oil used for this work.

Oil	Oil State	Speed of sound, V (T°C) (mm/µs)
Alpine	Fresh	$V = 1.587\ e^{-2.546^{-3}\ T}$
	5%	$V = 1.649\ e^{-3.806^{-3}\ T}$
	10%	$V = 1.606\ e^{-3.035^{-3}\ T}$
	15%	$V = 1.605\ e^{-2.174^{-3}\ T}$
	20%*	$V = 1.605\ e^{-2.174^{-3}\ T}$
HOOPS	Fresh	$V = 1.509\ e^{-2.689^{-3}\ T}$
	5%	$V = 1.502\ e^{-2.946^{-3}\ T}$
	10%	$V = 1.526\ e^{-3.415^{-3}\ T}$
	15%	$V = 1.501\ e^{-2.065^{-3}\ T}$
	20%	$V = 1.649\ e^{-4.165^{-3}\ T}$
Rock	Fresh	$V = 1.569\ e^{-2.387^{-3}\ T}$
	5%	$V = 1.589\ e^{-2.594^{-3}\ T}$
	10%**	$V = 1.635\ e^{-2.742^{-3}\ T}$
	15%	$V = 1.681\ e^{-2.890^{-3}\ T}$
	20%	$V = 1.673\ e^{-2.830^{-3}\ T}$

*Speed of sound could not be accurately measured for Alpine 20%, Alpine 15% was used for thickness calculations.

**Speed of sound was not measured for Rock 10%, so interpolation between Rock 5% and Rock 15% was used for thickness calculations.
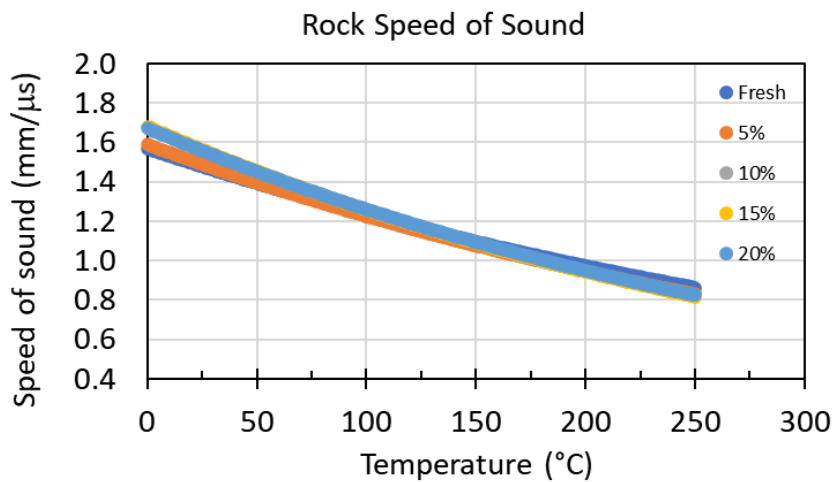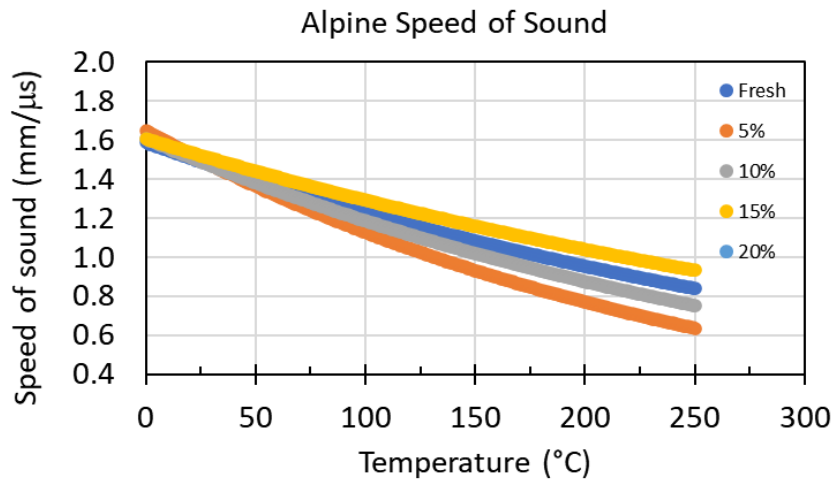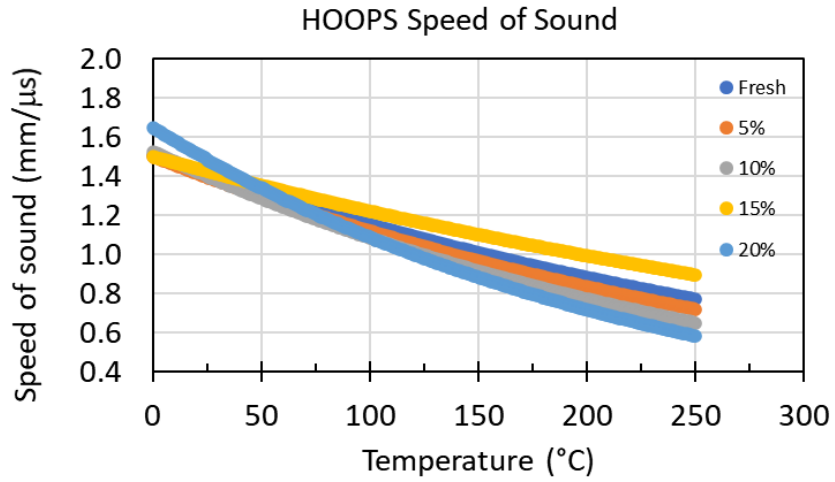
Figure 30. Speed of sound vs. temperature for HOOPS, Alpine, and Rock based on curve fitting to data.

4.6. Acoustic measurements of emulsion properties

An important outcome of this work was to show the proof of concept for acoustic measurement to identify and characterize emulsions. Acoustic waves can be used to characterize many materials including oils and water-in-oil emulsions. The acoustic waves interact with fluids in ways that allow measurement of the rheological properties of fluids. The propagation of an acoustic wave is described by a complex wavenumber, k, given by equation 1.

$$k = \frac{\omega}{V} + i\alpha \qquad\qquad 1$$

Where
ω is the frequency of the acoustic wave
V is the speed of sound in the fluid
α is the attenuation of the fluid

The speed of sound is related to the properties of the fluid through equation 2.

$$V = \sqrt{\frac{B}{\rho}} \qquad\qquad 2$$

Where
B is the bulk modulus of the fluid
ρ is the density of the fluid

The attenuation is given by equation 3.

$$\alpha = \frac{2\eta\omega^2}{3\rho V^3} \qquad\qquad 3$$

Where

η is the viscosity of the fluid.

The goal is to determine the ability of acoustics measurements to answer the following questions:

1. Is an emulsion present?

    a. Data from this work proves the ability to determine if an emulsion is present before and during ISB.

2. What is the water content?

    a. Proof of concept has been shown to the amount of water in lab settings has been shown lab settings

3. What is the droplet size distribution?

    a. Droplet size measurements suing acoustics ere not part of the scope of this project

4. Is the emulsion stable or changing?

    a. While acoustic measurements of the stability of emulsions were not part of the scope of the project we showed the proof of concept to determine the stability of tee emulsion by monitoring water droplet movement and separation.

4.6.1.1. Acoustic measurement of the presence of emulsion

In addition to the measurements on burning emulsions during this work that showed the ability to identify emulsified oil using acoustic sensors in the water under the slick, for this portion of the work we placed the sensors directly into the oil as shown in the left image of Figure 31. The resultant "sonar" image is shown in the right image of Figure 31. The sonar image is a combination of individual "pings". Each vertical line is an individual ping from the sensor located near the top of the liquid. The vertical axis is the travel time away from the sensor and the horizontal axis is the mixing time in seconds. The first region was fresh crude oil and the second region is the emulsion showing the scattering from the water droplets in the emulsion after 35 hours of mixing. These images clearly show the ability for acoustic measurements to identify that the oil has emulsified.
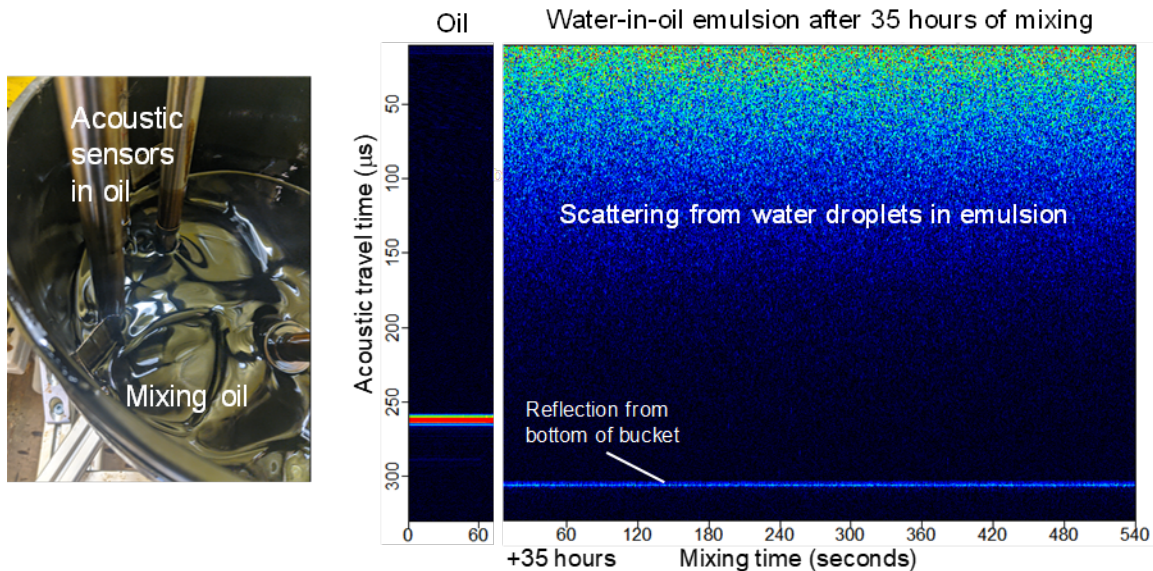
Figure 31. Acoustic measurements of oil before and after the formation of an emulsion.

4.6.1.2. Acoustic measurement of water content

Another property of emulsions that is important to measure is the water content. To test the ability of acoustics to measure the water content we measured the speed of sound and amplitude of the acoustic wave that was scattered back to the sensor as the water was added during mixing. It is important to note that this fluid was not a water-in-oil emulsion but rather a water-oil mixture to show a proof of concept of the physics and sensitivity to the water content. The acoustic sonar image during the addition of the water is shown in Figure 32. The time regions after the water was added are indicated by the water content (5%, 10%, 15%, 20%).

During addition of water
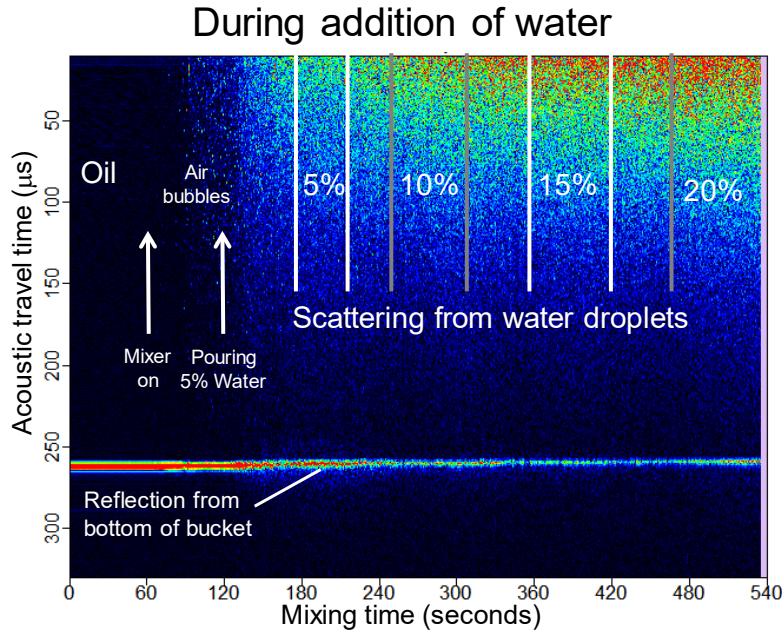
Figure 32. Acoustic measurement during the addition of water.

The resultant speed of sound and backscattering amplitude are shown in Figure 33 with the speed of sound plotted on the left axis and the backscattering amplitude plotted on the right axis. Both the speed of sound and the backscattering increased with the additional water. The increase in the speed of sound, V, is expected based on the rule of mixtures as shown in equation 4.

$$V_{fluid} = fraction_{oil}V_{oil} + fraction_{water}V_{water}$$ 4

At room temperature, the speed of sound of ANS is 1.362 mm/µs and the speed of sound of fresh water is 1.485 cm/µs. As expected the addition of water increased the speed of sound from the pure ANS towards the speed of sound of water. The backscattering increased as water as added because the mixing distributed the water into droplets increasing in number as more water was added. The data does show the proof of concept for measuring water content in water-oil mixtures and emulsions.
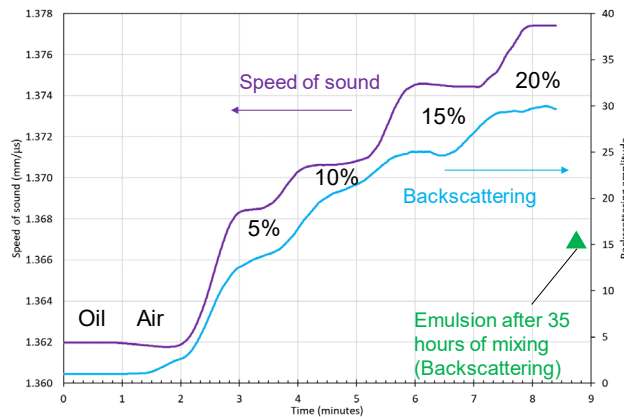
Figure 33. Speed of sound and backscattering during the addition of water

5. Small-scale ISB of Emulsified Oil

5.1. Small-scale ISB site setup

We performed 45 small scale burns on the three different oils shown in Table 5. Completion of these burns is a significant milestone for understanding ISB of emulsions across a large range of viscosities and water content. The check marks indicate 3 replicate burns for each state of oil. They ranged from a light oil, HOOPS, with a viscosity of 7 cSt at 20°C to Rock which has a viscosity of 2600 cSt at 20°C. To date we performed 45 burns on all three oils (HOOPS, Alpine, and Rock) and emulsions up to 20% water by mass as shown in Table 6. HOOPS and Alpine were evaporatively weathered ~15% by weight to increase the percentage of asphaltenes to enhance the stability of the emulsion. Rock was not evaporatively weathered as the resulting emulsification had high stability and obtained an optimal water droplet size distribution without that step.

Table 5. Properties of the oils and summary of test dates and parameters

	HOOPS	Alpine	Rock
Viscosity @ 20°C (cSt)	7	35	2600
Number of burns	15 (3 each state)	15 (3 each state)	15 (3 each state)
Date of burning	October	January	December

Table 6. Test matrix of burns. The checkmarks designate 3 replicate burns for each oil state.

| Oil state	HOOPS	Alpine	Rock
Fresh	✓✓✓	✓✓✓	✓✓✓
5% Emulsion	✓✓✓	✓✓✓	✓✓✓
10% Emulsion	✓✓✓	✓✓✓	✓✓✓
15% Emulsion	✓✓✓	✓✓✓	✓✓✓
20% Emulsion	✓✓✓	✓✓✓	✓✓✓

This series of burns was performed at West Metro Fire Training Center west of Denver, CO with a fire fighter on-scene to ignite the oil and to ensure safe burning. A 0.91 meter (36") diameter burn pan was used during the HOOPS ISB. For Rock and Alpine burns, a custom 1 meter diameter burn pan was used to ensure the burn rates and efficiencies were representative of larger burns and comparable to previous studies (see Figure 34). As with all our past burns, the 8 acoustic sensors were placed in the water to measure thickness and the 16 thermocouples were separated by 1 mm vertically to measure the temperature in the water, the oil, and above the oil. (see Figure 35). These burns create the science base for advancing the TRL of measuring the burn rate, efficiency, and oil volume in open water from mobile platforms.

Figure 34 Initial tank used for HOOPS burns (left) was exchanged for a 1 meter diameter pan (right) for Rock and Alpine burns.

Thickness (8 acoustic sensors)

Temperature inside slick (16 thermocouples)

Initial slick (10 mm)

1 mm
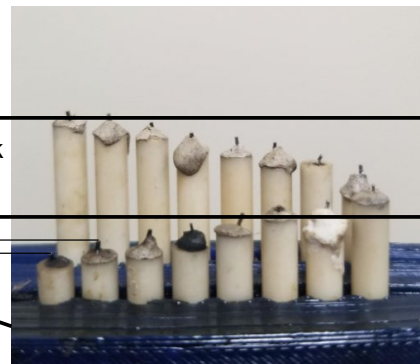
Acoustic sensors

Scale for in-situ weight
- Burn rate
- Efficiency

Figure 35. The thermocouple tree showing the 16 thermocouples in increments of 1 mm in the vertical direction.

The layout of the burn area and setup is shown in Figure 36. As in past burns, both stationary and moving cameras were used to capture the burn from several different angles and perspectives. Two cellphones were mounted to Wirals which allowed for back and forth movement above the burn pan. Two stationary cameras, an IDS machine vision camera and an

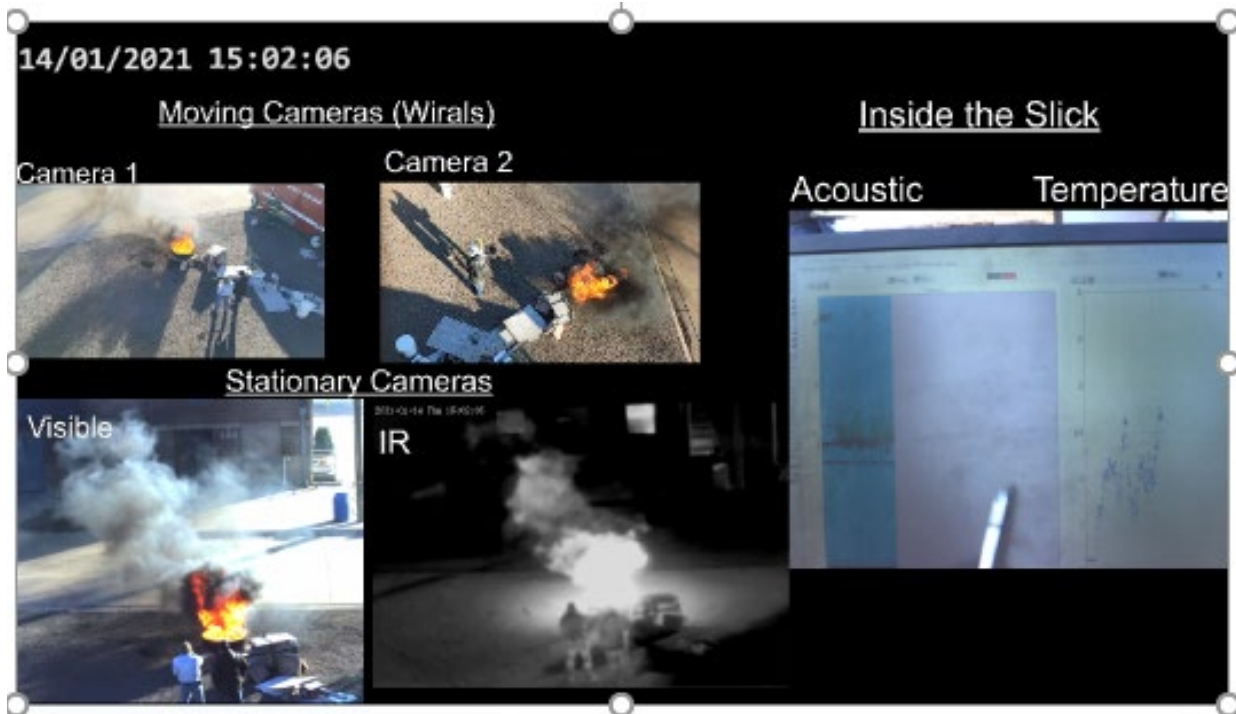infrared camera, were mounted to a nearby tower which allowed for a wider view of the entire burn scene.
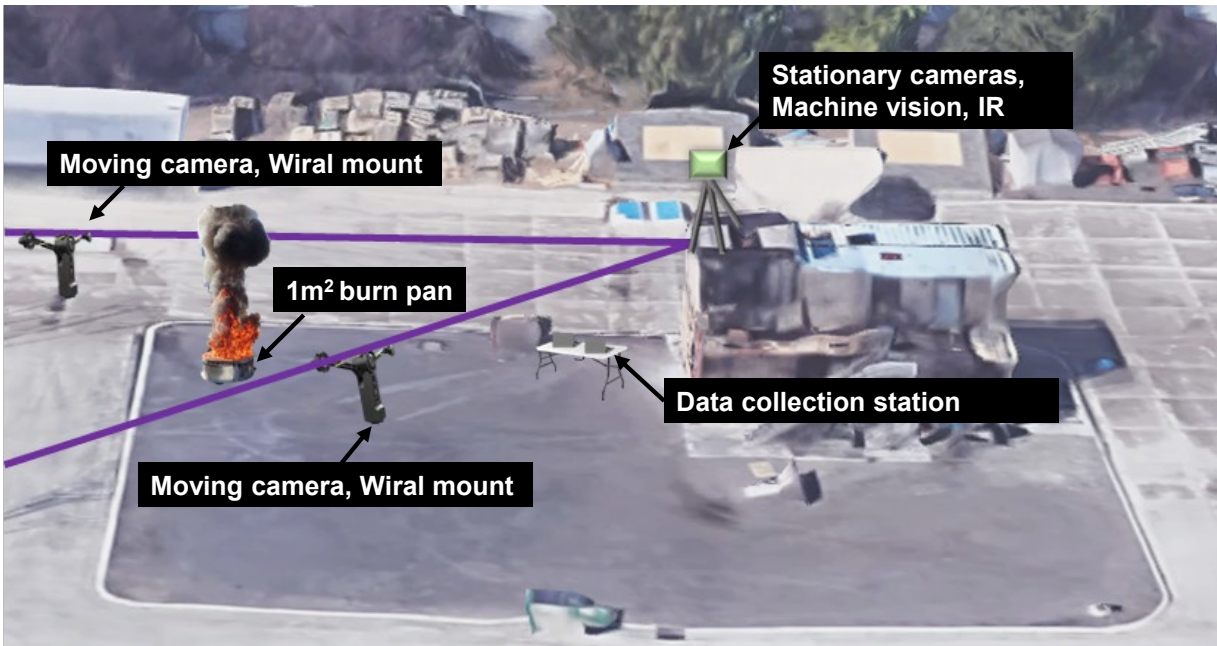
Figure 36. Layout of the burn area

A view of the simultaneous stream of all the cameras is shown in Figure 37.

Figure 37. Screen shot from video layout used for documenting the burns as well as for live streaming

The resultant sonar images are shown in Figure 38 for fresh HOOPS and the 10% and 20% emulsions. The resultant temperature profiles are shown in Figure 39. The solid blue line in the temperature profiles is from a faulty thermocouple. It was subsequently replaced for the burns on Rock.

The general behavior and features of the sonar images are similar to previous data. The sonar image from the fresh oil showed a region with steady burning from 100 seconds to about 250 seconds then boil over where the water evaporated through the slick and ejected water and oil into the air. The boil over of water is evident by the scattering for times later than the top of the slick. Visually this behavior looks like a "smearing" or "obscuring" of the top of the slick in the boil over region. For the emulsions the top of the slick is "obscured" through the entire burn since water is constantly boiling from inside the emulsion and ejecting water and oil into the air. This behavior increases in severity with increasing levels of emulsion. Some internal "structure" is evident in the emulsion due to the acoustic energy scattering from the water droplets in the emulsion (see white arrows). This behavior is subtle in these data because the settings for the acoustic system were optimized to observe the top and bottom of the slick rather than the internal structure. In subsequent burns for Rock the settings were adjusted on some of the sensors to highlight the internal structure in the emulsions.
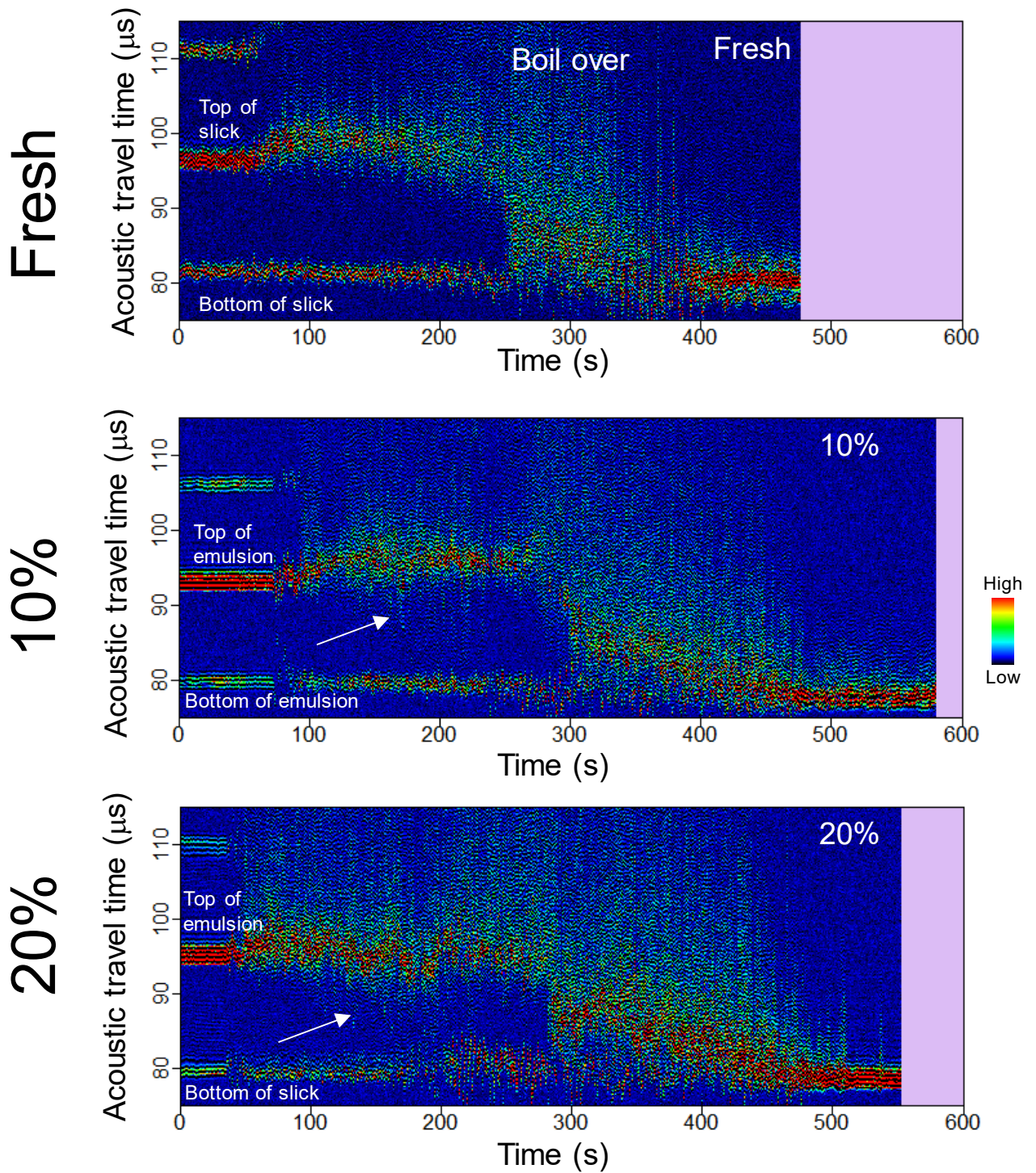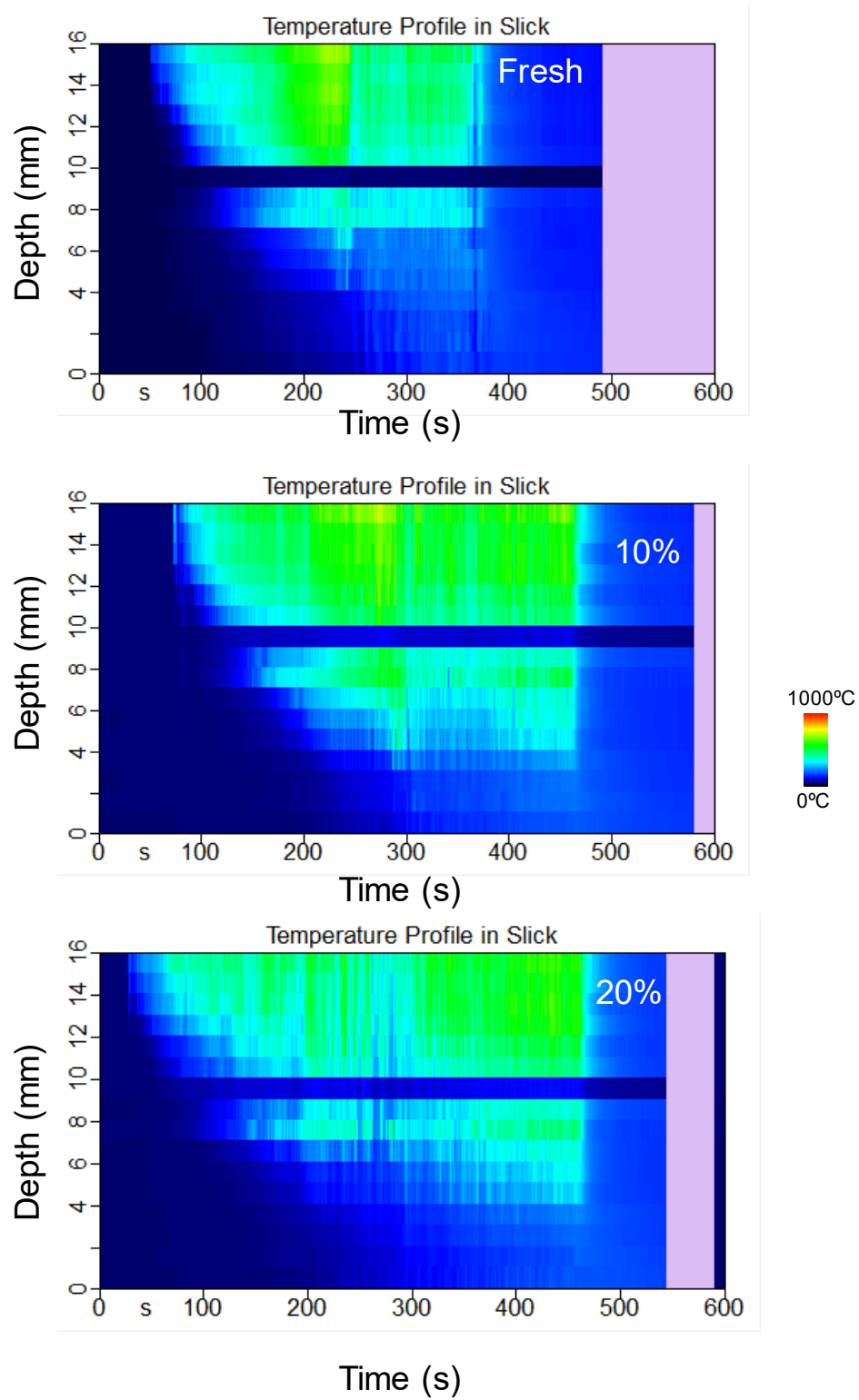
Figure 38. Sonar images from ISB of fresh alpine and 10% and 20% emulsions.

Figure 39. Temperature profiles in the slick from ISB of fresh alpine and 10% and 20% emulsions.

For all three oils, the duration of the burns generally increased with increasing water content, partially due to the need to burn off the diesel used for accelerant of the 15% and 20% emulsions. In addition to acoustic measurements, the entire apparatus was on a scale and mass was recorded in one second intervals. Measuring mass loss allows for a second method to calculate burn rate and mass loss. See Figure 40.
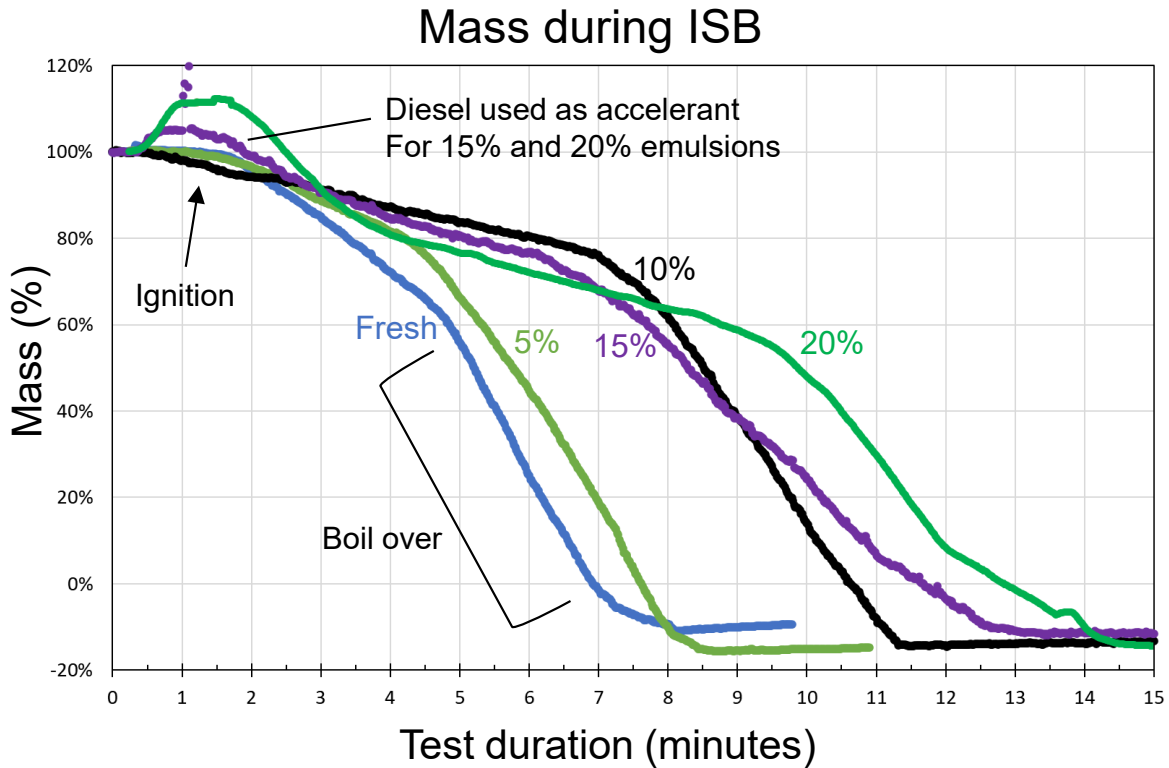
Figure 40. Mass loss of Rock for fresh and emulsified oils up to 20% water content.

By comparing the mass loss measured with the scale with the acoustic data we determined the thickness of the slick during ISB. We used a harmonic mean approach to measure the thickness in manner similar to the previous phase [3]. In this phase the analysis was automated to the degree that all data from 45 burns were analyzed with one piece of software with one command. The resultant thickness as a function of time for fresh and emulsified HOOPS and Rock are shown in Figure 41 and Figure 42. The blue line is the thickness from the acoustic measurements and the greenish-yellow line is the thickness from the scale. Agreement is excellent prior to boil over where the burn rates were calculated.

HOOPS
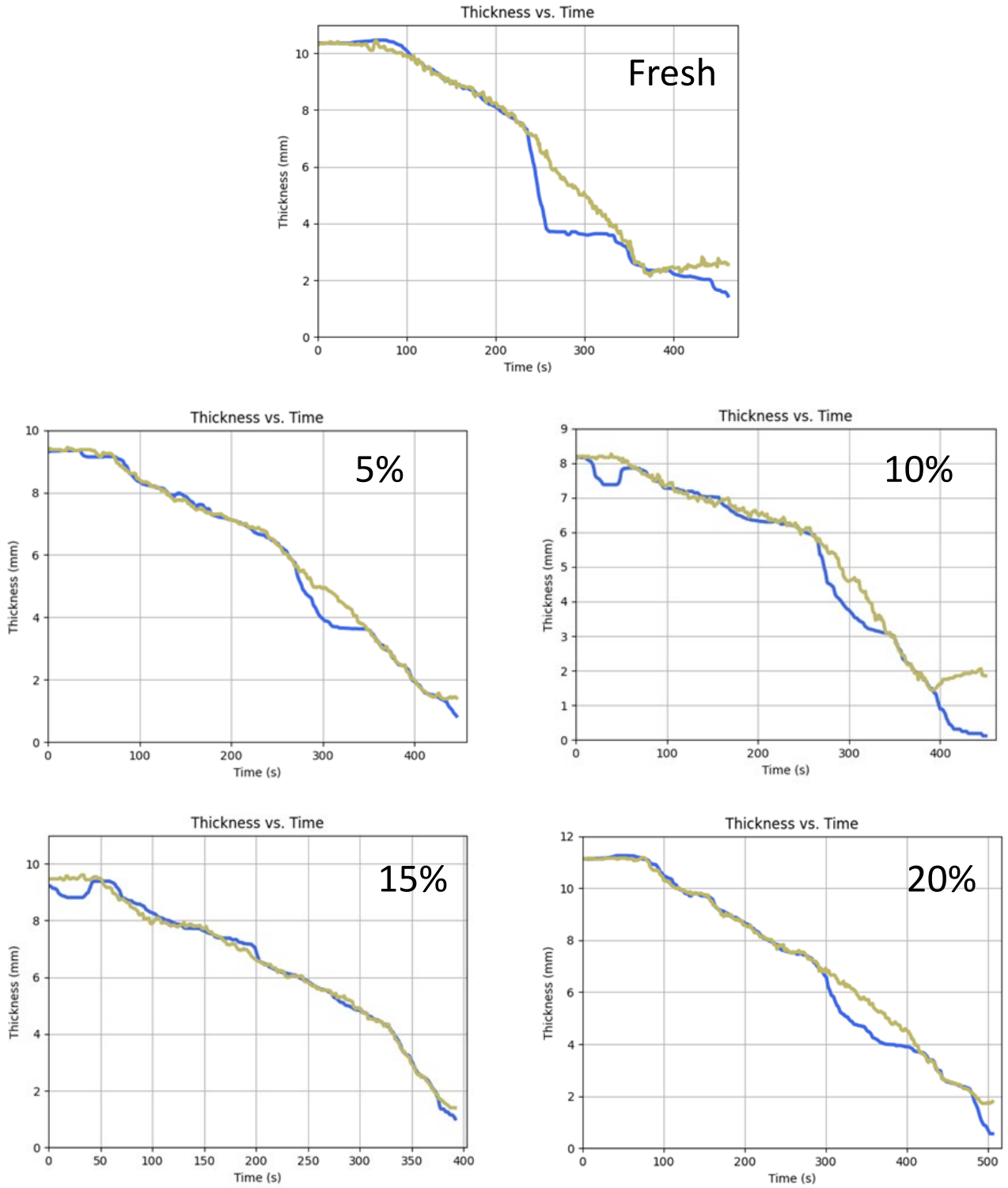
Figure 41. The thickness during the burning of HOOPS. The thickness from the acoustic measurements is shown in blue and from the scale shown in greenish-yellow.
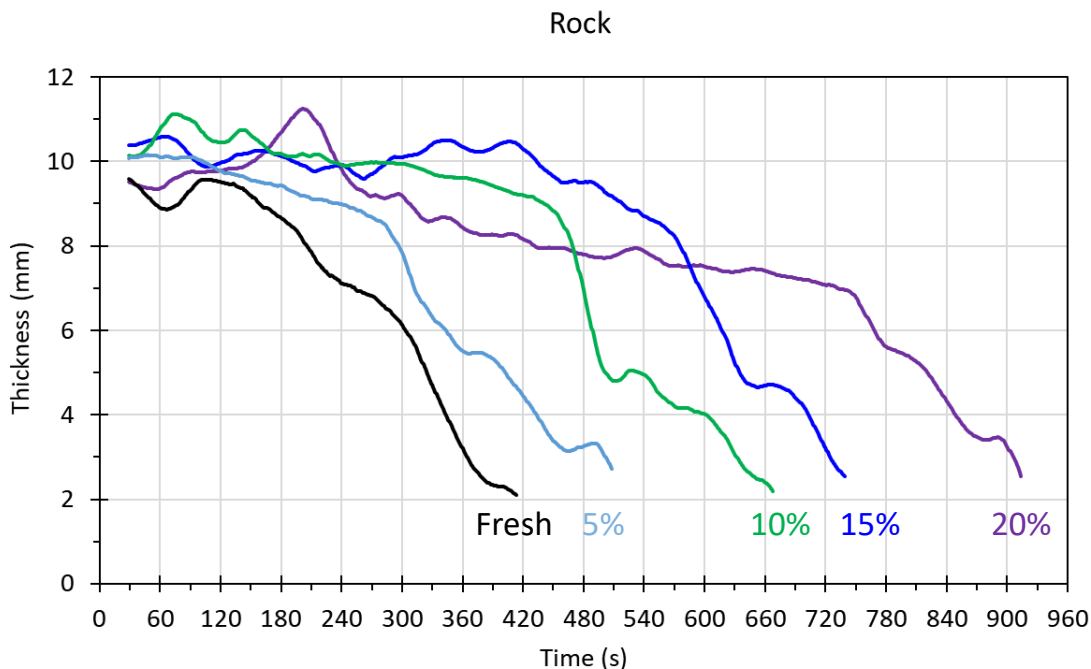
Rock
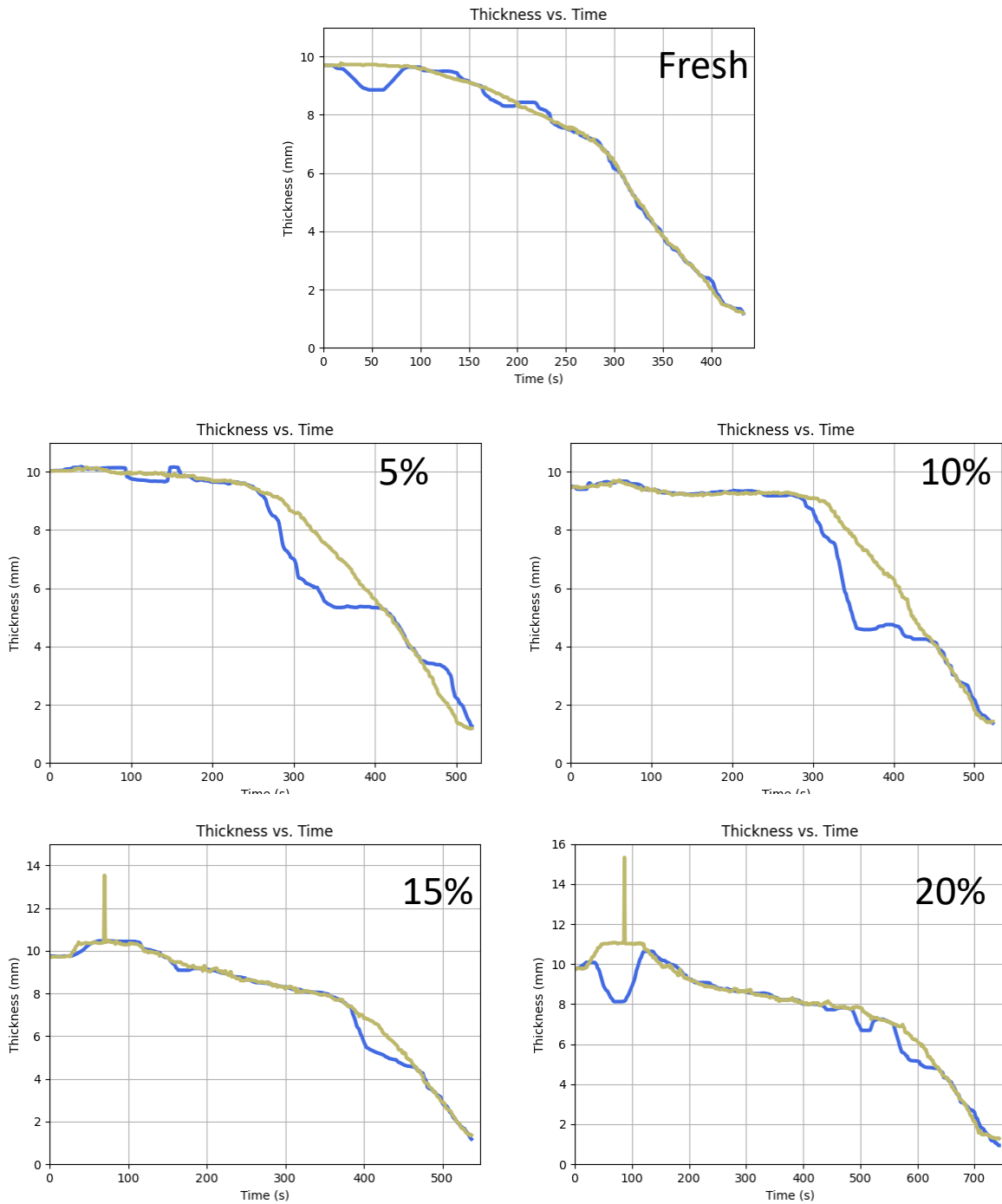
Figure 42. The thickness during the burning of Rock. The thickness from the acoustic measurements is shown in blue and from the scale shown in greenish-yellow. The spike in the curve from the scale occurred when the torch used to ignite the fire was pressed onto the apparatus and was used as a fiducial marker to indicate initiation of the ignition.

To emphasize the different in burning rates and time for Rock the thickness from the acoustic measurements is plotted on one graph shown in Figure 43. The fresh oil burned rapidly, and the burning time increased with increasing levels of emulsification. These data emphasize the need to measure the thickness continuously during burning so that the region prior to boil over can be distinguished from the boil over so that the burn rate can be accurately measured. The burn rates can be significantly overestimated if a line is simply connected from the beginning of the burn to the end of the burn.
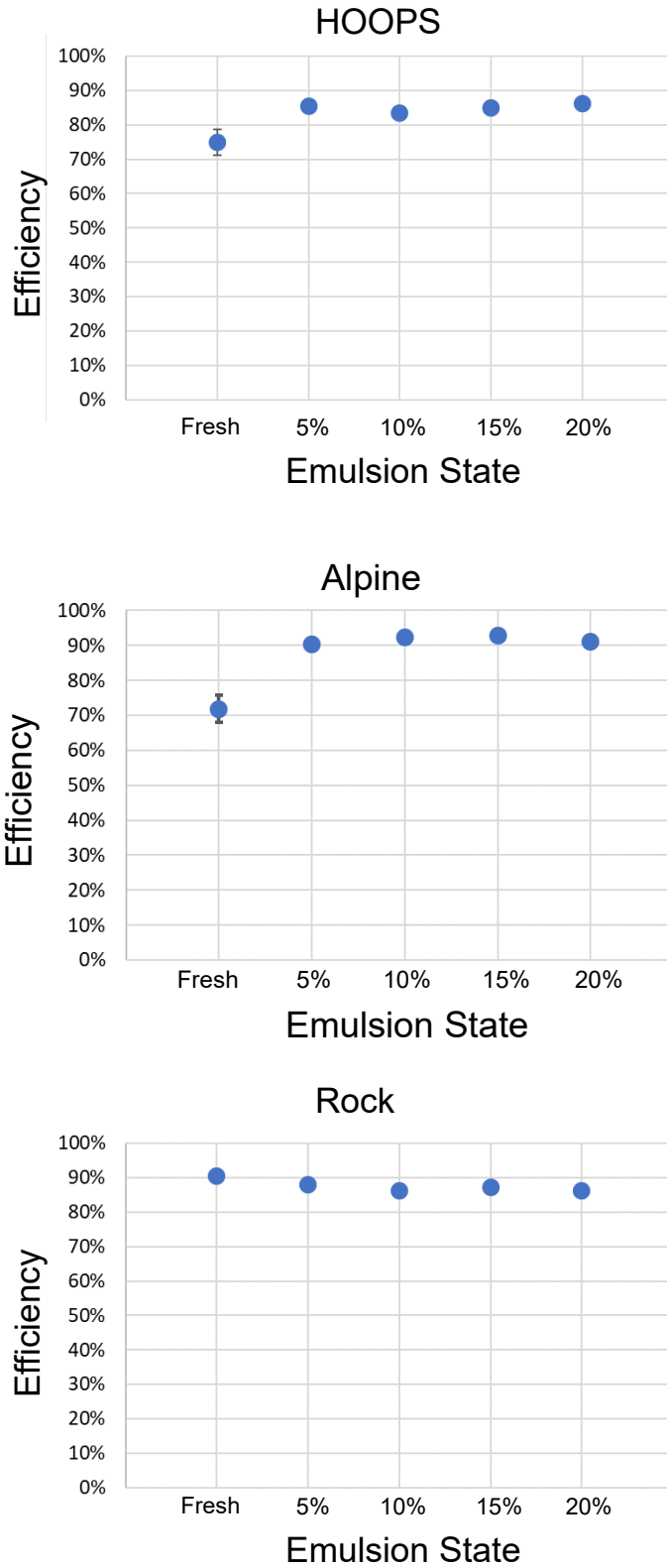

Rock

Figure 43. The thickness of oil from acoustic measurements for fresh Rock and for emulsions up to 20% water.

The burn rates were determined during the time region before boil-over and after the diesel burned off for the 15% and 20% emulsions. Figure 44 shows the burn rate for HOOPS, Alpine, and Rock for fresh and emulsified oils up to 20%. The error bars represent the standard error for the three replicate burns. The burn rate for HOOPS decreased slightly as the level of emulsification increased then increased for the 20% emulsions. The burn rate for Rock decreased significantly from ~1 mm/min for fresh Rock to ~0.4 mm/min for the 20% emulsion. The burn rate for Alpine behaved dramatically different as the level of emulsification increased. The burn rate first increased from fresh to 10% water content then dropped for 15% and 20%. Unlike previous oils, Alpine generated foam after ignition. Often the foam was so thick that it would block the oxygen necessary for burning and extinguish the fire. We had to reignite the Alpine multiple times due to the foam extinguishing the flames. The slightly elevated burn rates from the 15% and 20% emulsion for HOOPS and Rock may be due to the addition of diesel as an accelerant. In future burns it may be desirable to use the same amount of accelerant for all burns including fresh so that the rates can be directly comparable. Even with this uncertainty, it is clear the burn rate decreases dramatically with increasing levels of emulsification. The corresponding efficiencies of the burns are shown in Figure 45. The emulsification level had a much less dramatic effect on the efficiency as compared to the burn rate with the efficiency

increasing for HOOPS and Alpine as the level of emulsification increased, but the efficiency decreased for Rock as the level of emulsification increased.
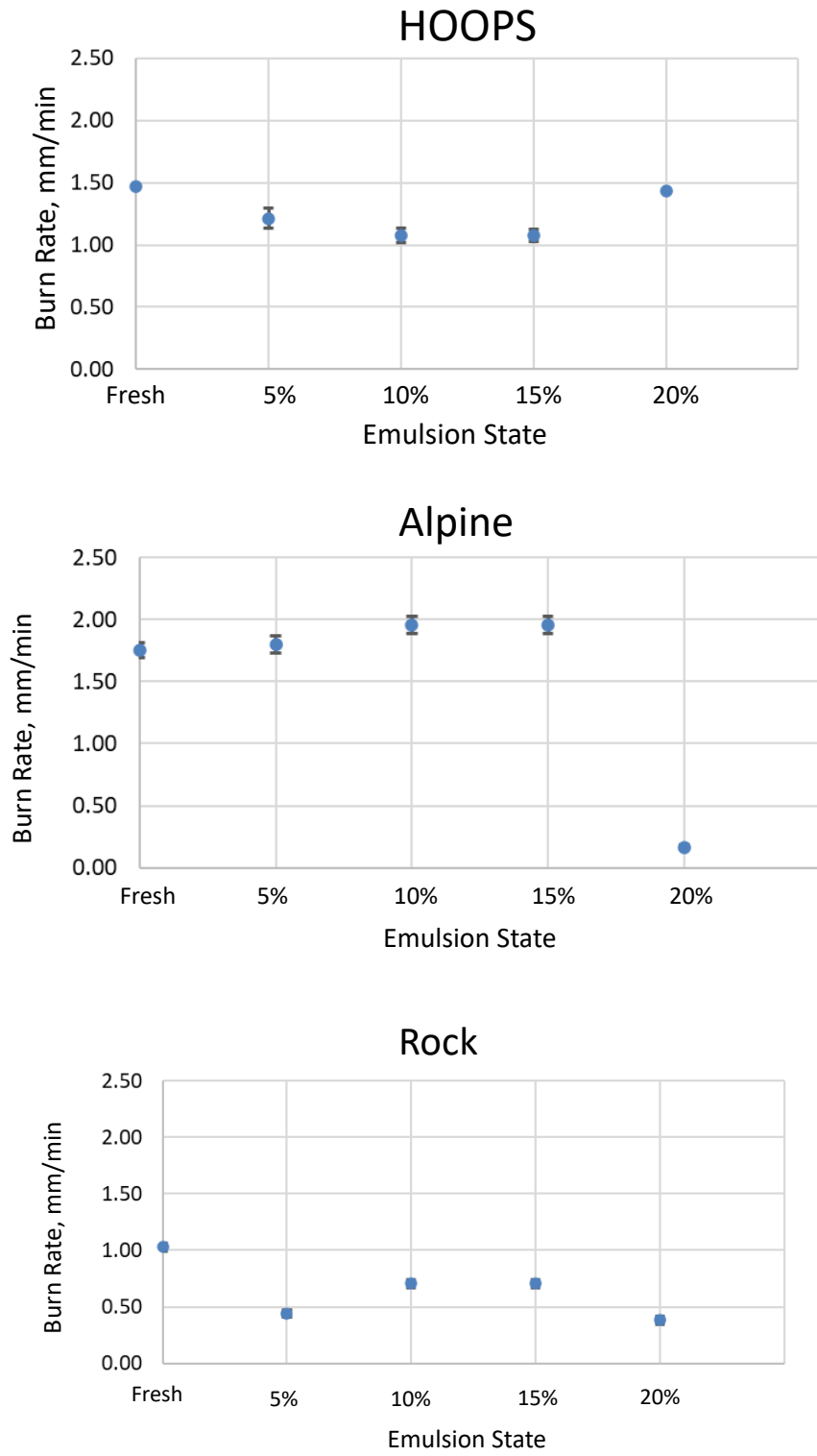
HOOPS

Alpine

Rock

**Figure 44. Burn rate as a function of emulsification for HOOPS, Alpine, and Rock from mass loss.**

Figure 45. Efficiency as a function of emulsification for HOOPS, Alpine, and Rock from mass loss.

6. Meso-scale ISB of fresh oils

6.1. Meso-scale set up

Twenty mesoscale burns were performed at the North Metro Fire Training Center, just north of Denver, CO. An overhead schematic of the burn site is shown in Figure 46. We constructed a 20 foot x 20 foot x 5 foot deep structure using large landscaping blocks. The bottom was filled with sand and then lined with a commercial pond liner to hold the water. Two boom designs were fabricated using sheet metal and supported by custom-made stands that allowed the boom to be shaped as desired and moved vertically as needed. Chains were used to fasten the boom support structures to the wall to further stabilize the boom and ensure that it did not shift unexpectedly or fall during operations. Pictures of the tank and boom are shown in Figure 47 and Figure 48. To simulate a flowing current, ice eaters were placed at the opening of the boom and controlled individually with a variable voltage control source (Variac).
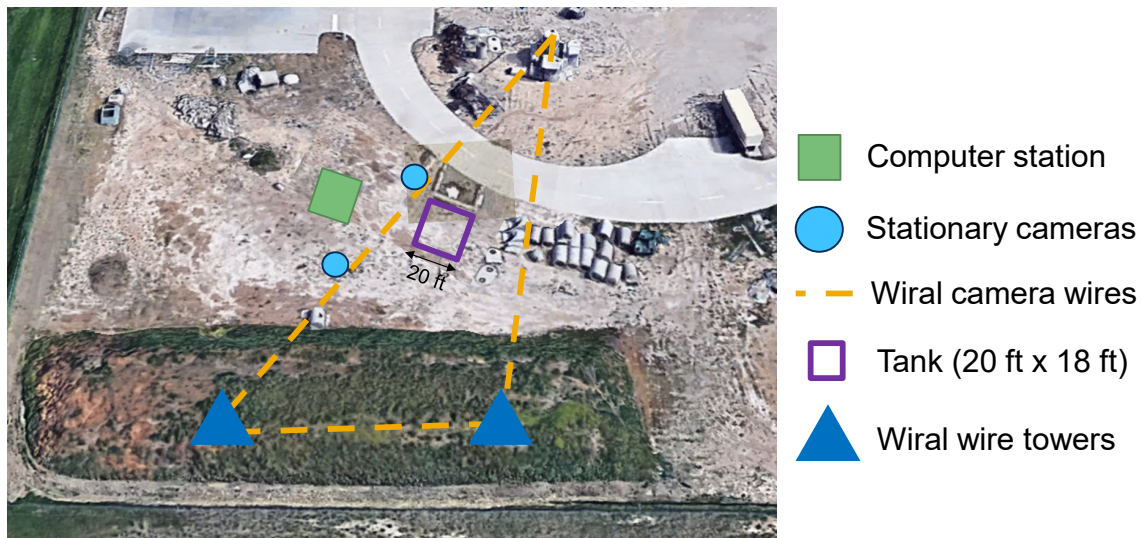
Figure 46. Burn site at the North Metro Fire Training Center near Denver, CO.

*Figure 47. Finished tank with sand layer and pond liner.*

Figure 48. Boom in configuration 1 prior to installation of sensors.

The boom was configured into two different shapes, as shown in Figure 49. Mechanical drawings of parabolic (left) and U-shaped (right) booms., to test the effects of containment: a parabolic-like design and a U-shaped design. The single boom lasted through 20 burns with no sign of degradation or damage. It was found that for the distance the ice eaters were from the opening of the boom each ice eater could control flow over ~ 1 m across the boom opening. Flow rates were estimated to be ~0.5 knots to ~0.75 knots during burning, based on the movement of floating orange peels on the water. The freeboard was maintained at ~4 inches and was adequate for these flow rates. During high wind events, higher flow approximately 1 knot or more were periodically needed to keep the oil and flames contained.
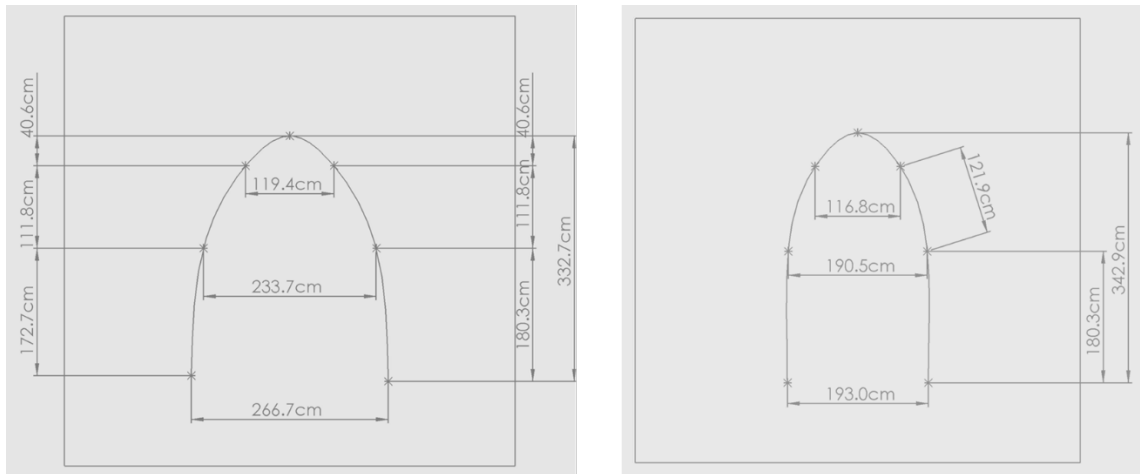
Figure 49. Mechanical drawings of parabolic (left) and U-shaped (right) booms.

Multiple cameras were used to record the burns as shown in the schematic in Figure 46. The cameras included two visible cameras placed on moving cable camera systems (Wirals), stationary visible cameras, and a stationary IR camera. The configuration of the thermocouples and acoustic sensors is shown in Figure 50. The acoustic sensors were spaced to allow collection of thickness of the oil throughout the burn over a large area. The thermocouples were spaced 1 mm vertically and were placed so that the temperature inside the slick as well as above and below the slick could be measured. On most burns videos from a hand held cell phone camera were recorded as well. Twenty eight unique sets of data and videos from the 8 acoustic sensors, 16 thermocouples, and videos from the 4 cameras was synchronously streamed directly to the computer hard drive.
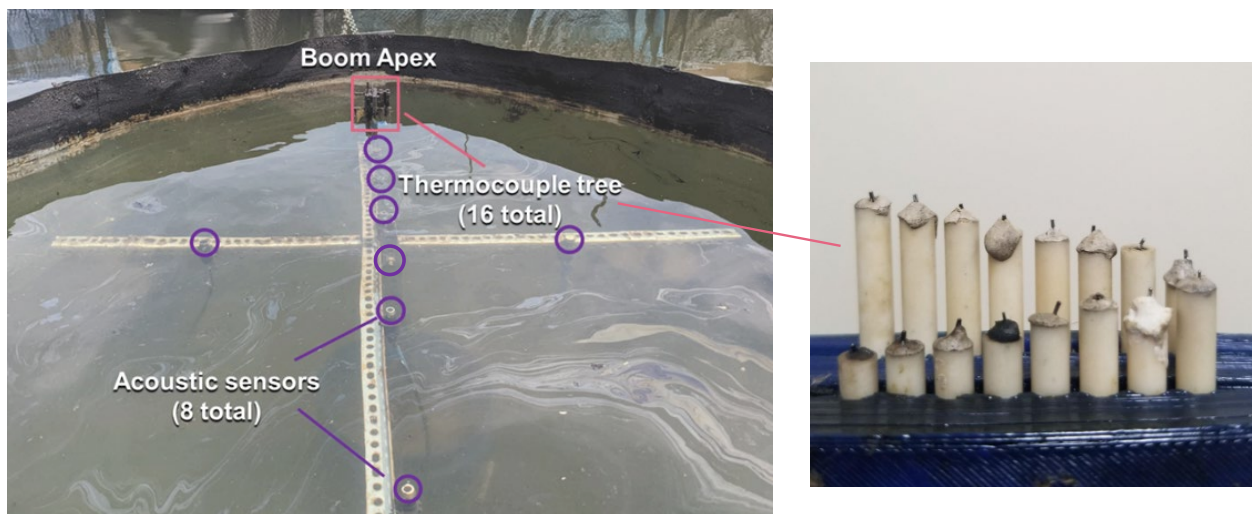
Figure 50. Acoustic and thermocouple sensors in the boom

6.1.1. Acoustic data collection

Acoustic sensors were mounted to a rigid structure, primarily along the length of the boom, to measure variable slick thickness. Measurements were initially going to be collected using sensors mounted on a ROV, however, the ROV enclosures were leaking water so we opted to use the static sensor mount. The benefit of using fixed acoustic sensors with known locations both these sensors and the thermocouple tree is that it allowed for direct comparison with our small-scale burns. They will also allow the ROV measurements to be benchmarked for future large-scale burns. Additionally, the data collected on hydrodynamics and variation of the slick thickness close to the boom could be used to influence boom design and provide insight on the relationship between thickness variation in the boom, burn rates, and efficiency.

6.1.2. Aerial imaging and surface area algorithm development

Initially in the mesoscale burns, two Wiral-mounted cameras were used to obtain comparable footage to that collected using drones in the field, however, due to ambient temperatures, which exceeded 100°F, and radiant heat from the fire, the Wiral-mounted cameras overheated and shut down almost immediately. An iterative approach was taken to delay overheating of the Wiral-mounted cameras so they could last through an entire burn. The final design consisted of placing a single cell phone in an insulated pouch along with an ice pack and an aluminum foil shield. This method allowed operation during most mesoscale burns; however, future use of a UAV would eliminate these issues.

Overall, streaming to OBS worked very well. There was a high frame rate when a single Wiral-mounted camera was used, however the framerate dropped substantially when three Wiral-mounted cameras were used. During future burns, the use of multiple wireless routers could help maintain high framerates if Wirals and cell phones are used. UAV mounted cameras would eliminate this issue.

A trial deployment of the Xbee radio control system was planned for the meso-scale burns with a prototype Wiral. The high temperatures onsite and resultant overheating of Wiral-mounted cameras forced this plan to be abandoned. The cameras required insulation modifications and constant monitoring. The Xbee control also require constant attention, making simultaneous management of camera heat exposure and Xbee control deployment impossible. As the camera system can be hardened outside the time during the mesoscale burns, the decision was made to prioritize quality video recordings to support the higher priority area computations.

6.2. Meso-scale ISB test matrix

For the first time the volume of the burning oil as a function of time has been calculated and used to determine burn rates and efficiencies. The mesoscale burns were especially productive with work starting from an empty lot and culminating with 20 burns with volumes of oil ranging from ~ 3 gallons to over 9 gallons. The mesoscale burns were designed to provide data on the scaling for the burn rate and efficiency through comparison with our data from the 1 m diameter pan. They also served as a testing ground for oil handling and fire containment for larger scale burns. Table 7 shows the burns completed. We had seven active days of burning and could turn around the burns as quickly as 1 per hour. To compare with the burn rates and efficiencies

of the small scale burns we focused analysis on HOOPS, Alpine, and Rock.

Table 7. The 20 meso-scale burns were performed for 8 different oils, with the volume of oil used ranging from approximately 3-9 gallons. Each check mark indicates a burn replicate.

| Approximate Volume Burned (gallons)	Thunderhorse	ANS	Canadian Sour Crude	Agbami	HOOPS	Alpine	Rock	Platform Gina
3			✓					✓✓
5	✓	✓		✓	✓✓✓✓	✓	✓	
7		✓			✓✓✓		✓	
9	✓							

6.3. Meso-scale ISB results

One of the main goals of this project is to scale up the ISB measurement technology from small scale to large scale. These mesoscale burns served as an excellent opportunity and source of data to compare burn rates and efficiencies across a large length scale and oil volume range. Specifically, the 45 small scale burns performed used approximately 2 gallons of oil per burn in a small burn pan that ranged from 0.9 meters diameter with an area of 0.64 m^2 to a 1 meter diameter pan with a corresponding area of 0.8 m^2. In contrast these mesoscale burns ranged from 5 gallons to 7 gallons in volume with burns that attained a surface area as large as 4.5 m^2. To allow direct comparison between the small scale and mesoscale we focused on the three oils used in the small-scale testing, Alpine, HOOPS, and Rock. Images from the videos recorded are shown in Figure 51, Figure 53, and Figure 55. The "Sonar" image obtained from the acoustic sensors and the temperature inside the slick for these mesoscale burns are shown in Figure 52, Figure 54, Figure 56. For each burn the slick was ignited approximately 30 seconds after data collection was initiated. The undulations in the slick of Rock seen in Figure 56 show a direct indication of the action of the ice eaters causing the slick to increase and decrease in thickness as their power was adjusted higher and lower. The area and thickness of the slicks were changing continuously during the burn to help simulate open water

environments. In general, the acoustic signals looked similar to those seen in the static small-scale burns but moved quite a bit as the slick changed size and shape.
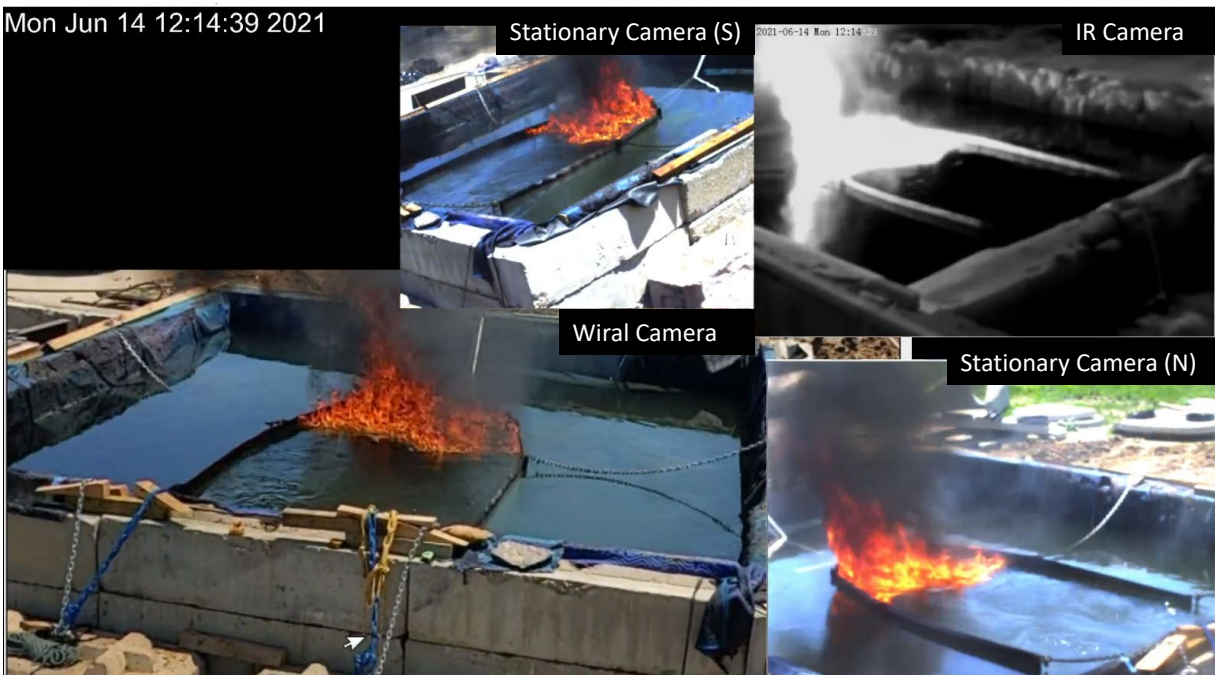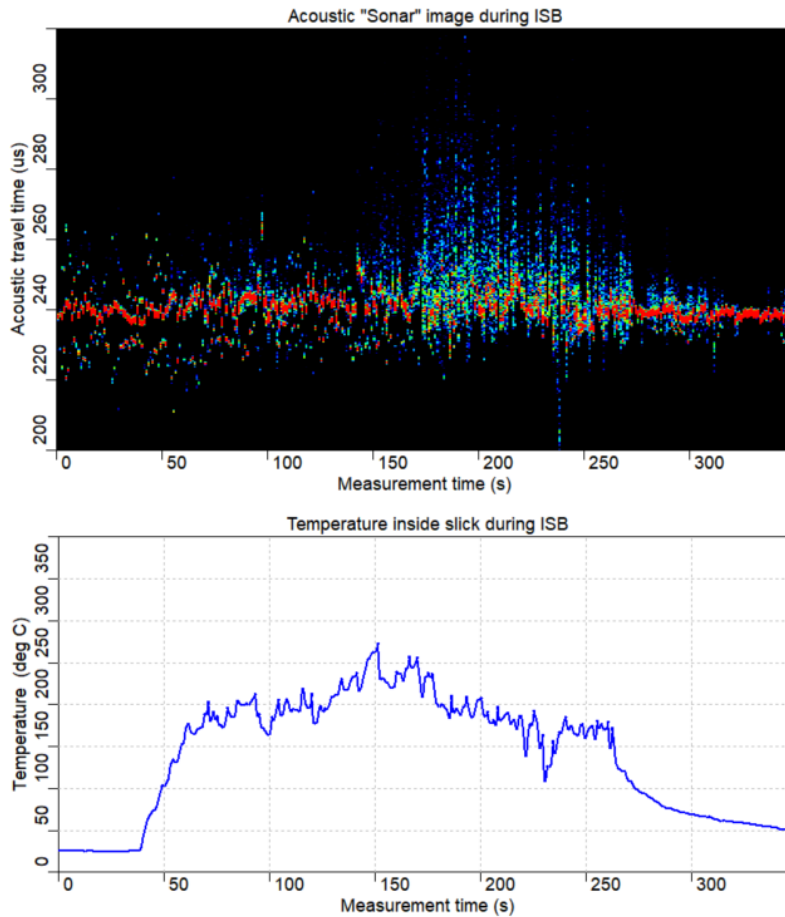

Figure 51. Images of the burning Alpine from moving and stationary visible light cameras as well as an IR camera.
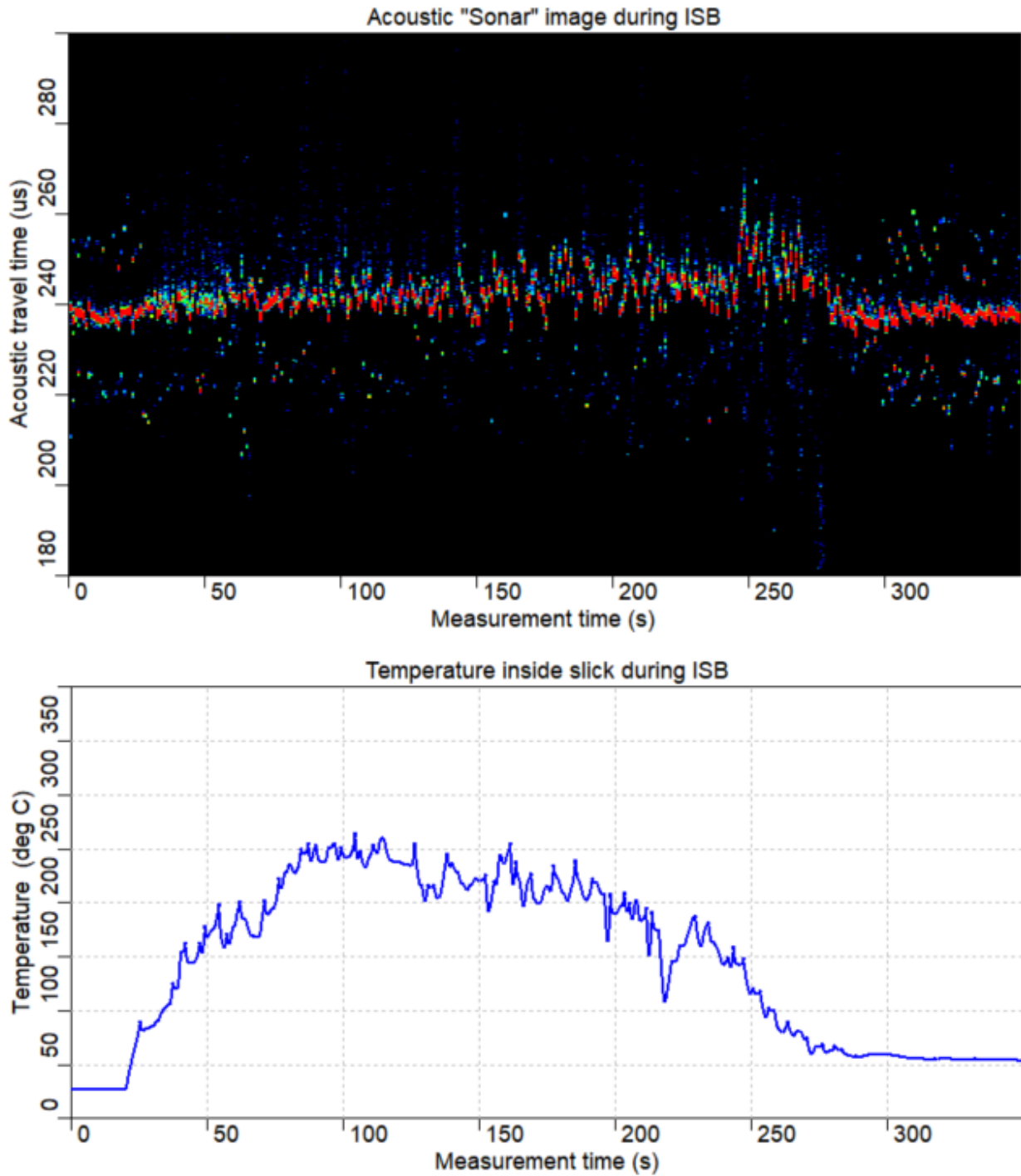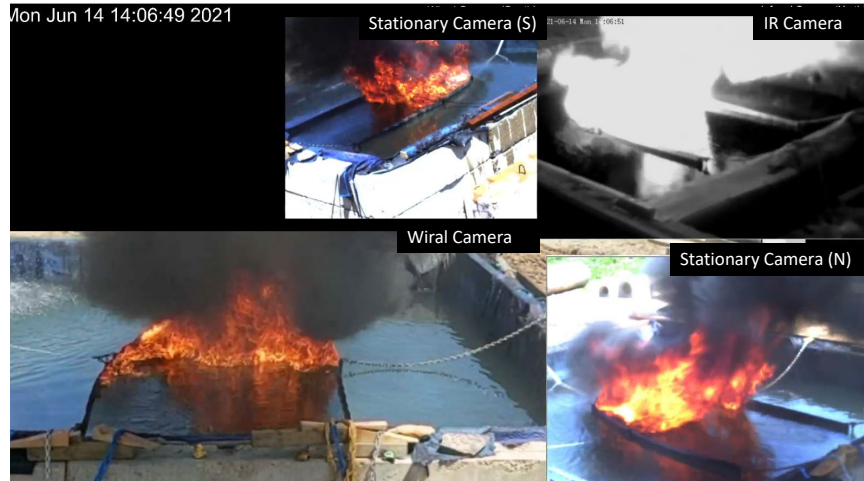
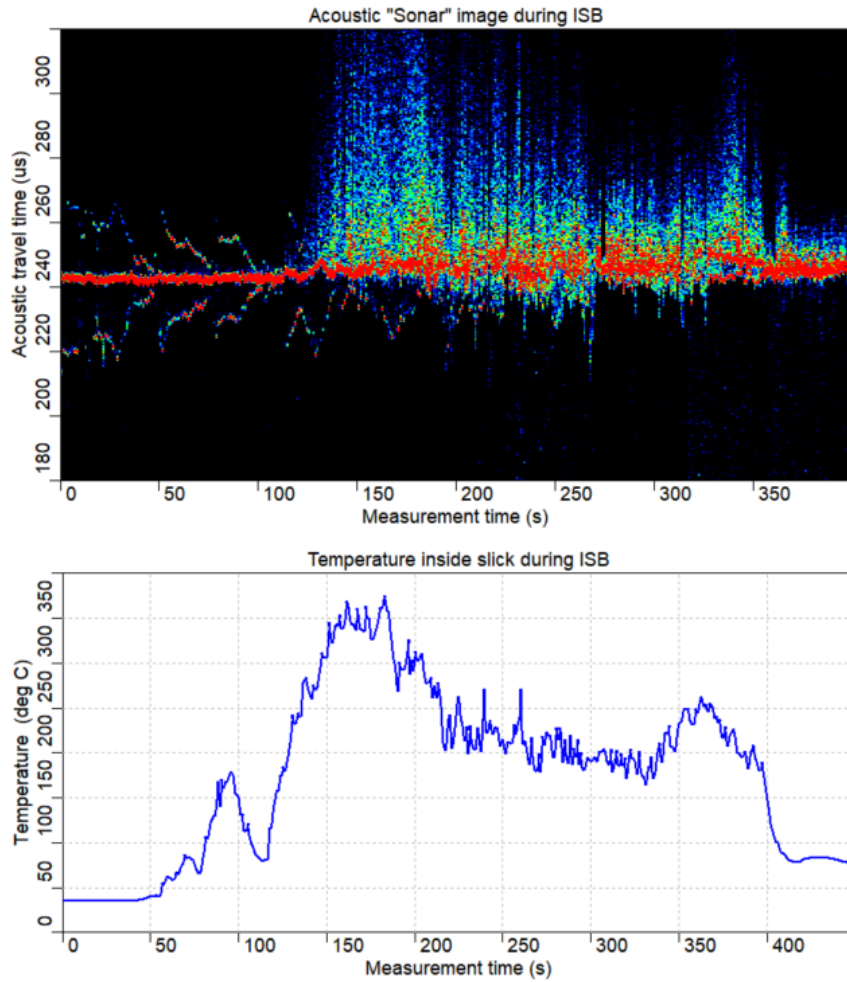**Figure 52.** *Acoustic sonar image and temperature inside the slick during burning for Alpine.*

Figure 53. Images of the burning HOOPS from moving and stationary visible light cameras as well as an IR camera.

*Figure 54. Acoustic sonar image and temperature inside the slick during burning for HOOPS.*

*Figure 55. Images of the burning Rock from moving and stationary visible light cameras as well as an IR camera.*

Figure 56. Acoustic sonar image and temperature inside the slick during burning for Rock.

6.4. Volume of oil during ISB

The corresponding surface area, thickness, and volume during the burning are shown in Figure 57, Figure 58, and Figure 59. The surface area and thickness were calculated from the aerial videos and acoustic measurements respectively. Combing the thickness and area to obtain a volume of burning oil during ISB is the first time a direct measurement of the volume of oil for burning oil in a semi-contained space as far as we know. The ability to directly measure the volume of oil is a first of a kind measurement capability that will allow the oil spill response community to know the volume of oil on the water and the amount of oil burned with unprecedented accuracy.
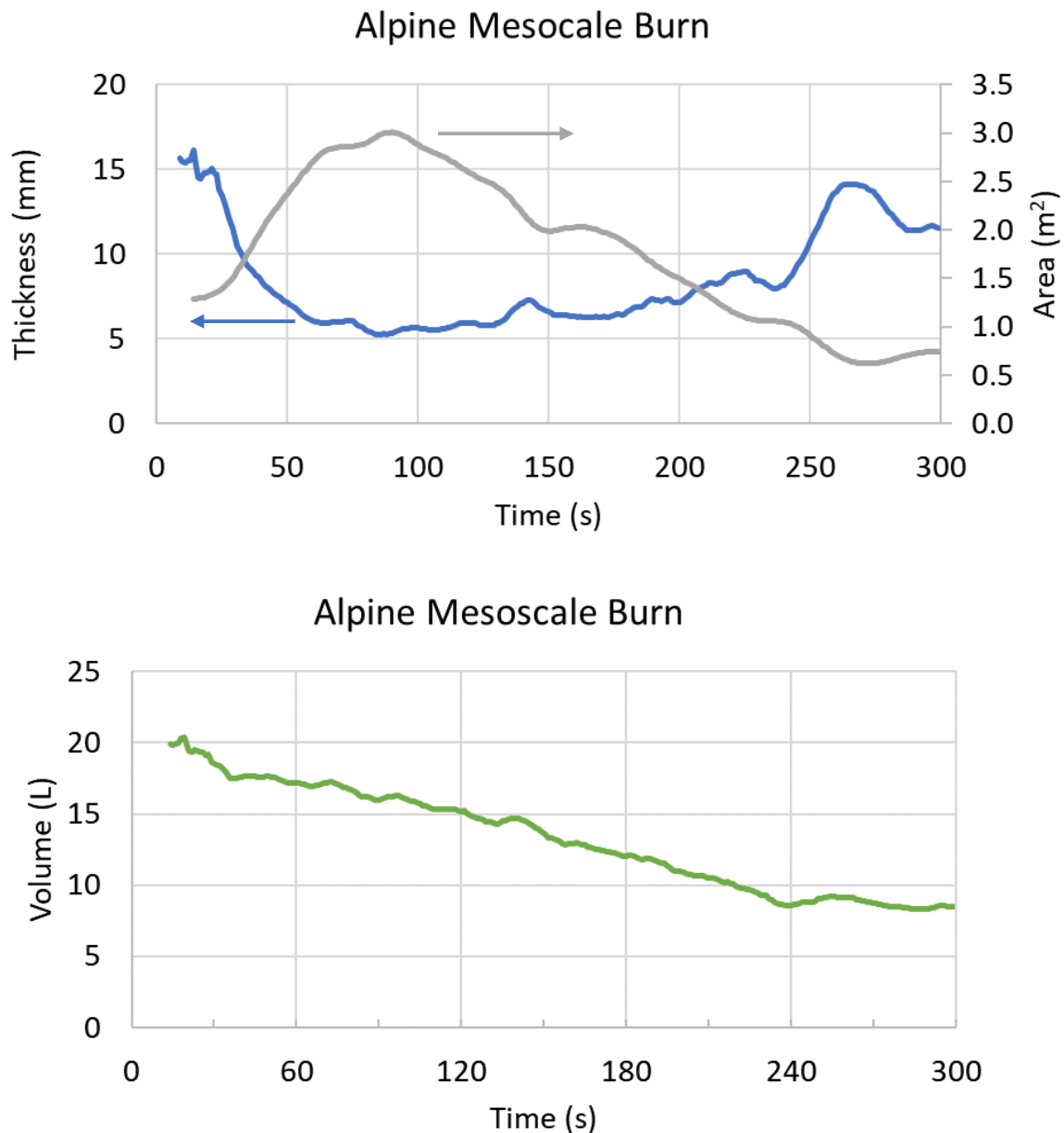
Figure 57. Area, thickness and resultant volume during ISB of Alpine.
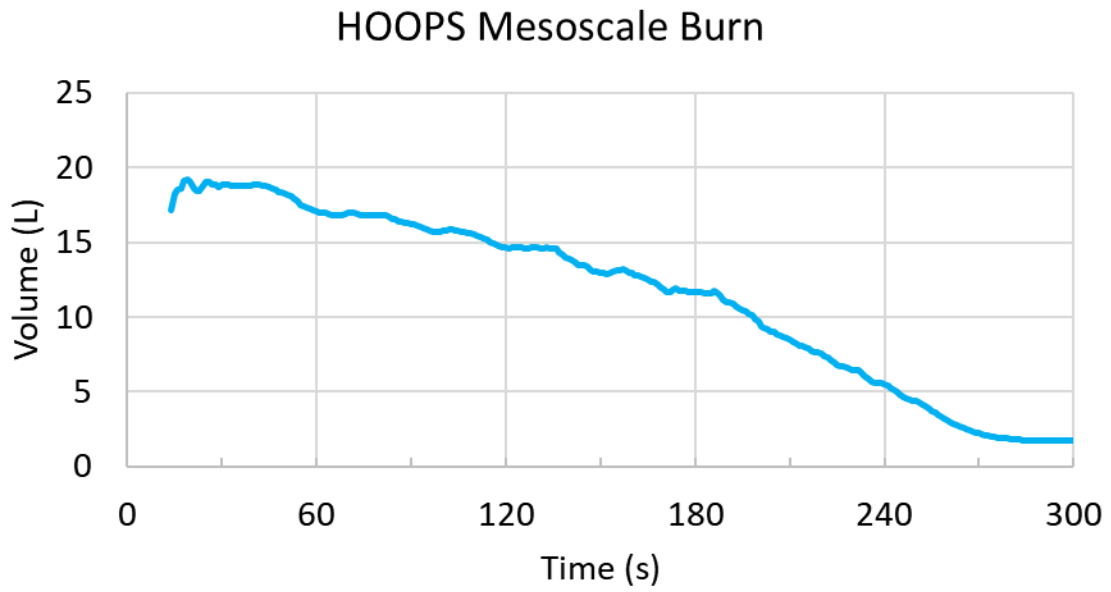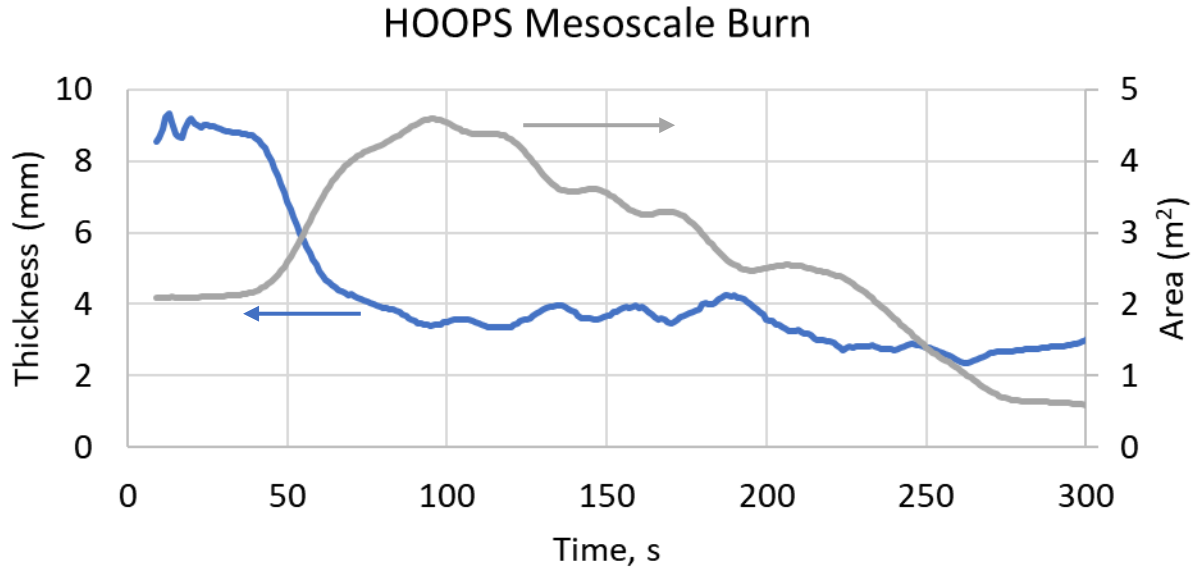
Figure 58. Area, thickness and resultant volume during ISB of HOOPS.
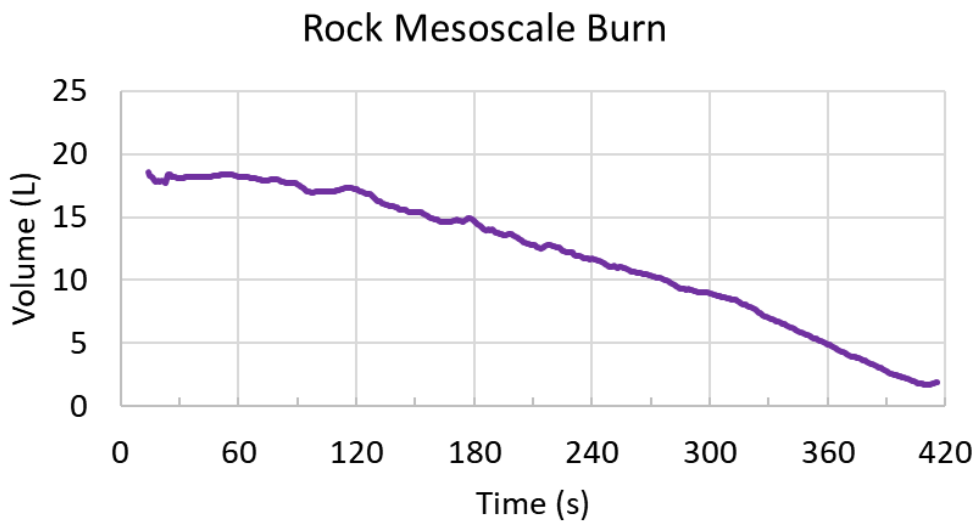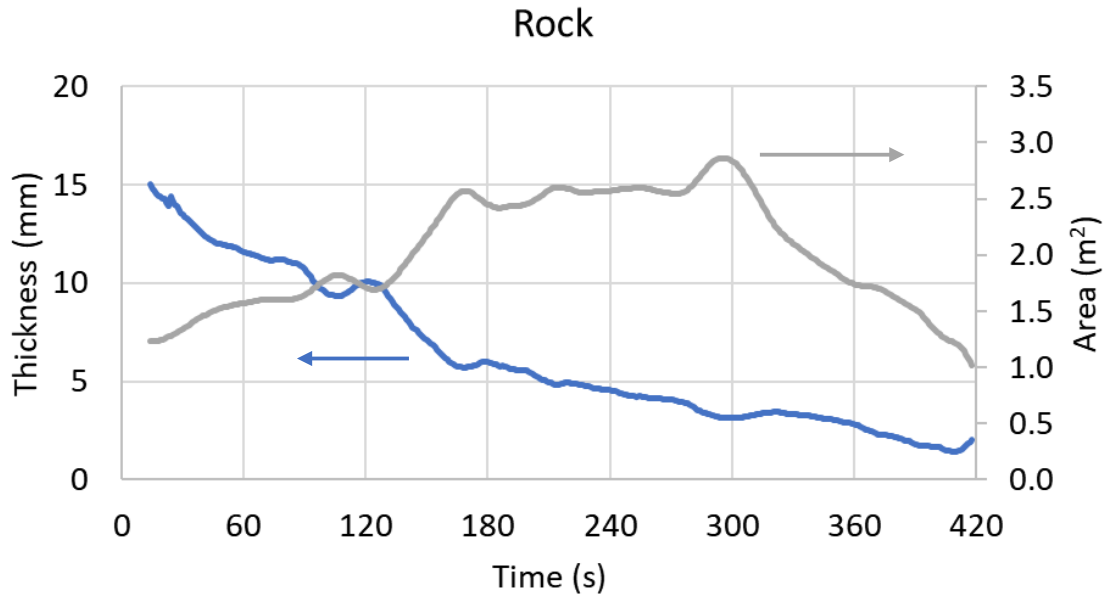
Figure 59. Area, thickness and resultant volume during ISB of Rock

Using the data collected the burn rates for the small scale and mesoscale burns were calculated as shown in Table 8. The burn rates for mesoscale burns of Alpine and Rock are very close between the two scales with HOOPS showing a reduction in burn rate as the size increased to the mesoscale.

Table 8. Burn rate of small scale and meso scale burns of fresh oil.

Burn rate (mm/min)

Oil State	Alpine	HOOPS	Rock
Small Scale	1.75	1.47	1.03
Meso Scale	1.43	0.76	1.10

The efficiency for the burns from the small scale to the large scale were comparable (Table 9) with Alpine having the lowest efficiency for both the small scale (72%) and the meso scale (60%). HOOPS had a 75% efficiency for the small scale and a 90% efficiency for the mesoscale and Rock was 88% efficient for the small scale and 90% efficient for the mesoscale. We are further analyzing the data from the HOOPS mesoscale burn to determine if the degree of vigorous burning during boil over could have affected the burn rate and efficiency.

Table 9. Efficiency of small scale and mesoscale burns of fresh oil.

Efficiency

Scale	Alpine	Hoops	Rock
Small Scale	72%	75%	88%
Meso Scale	60%	90%	90%

7. Conclusions

This project made significant advancements to the ability to directly measure the volume of oil in the environment and specifically during ISB. The technology advanced into TRL 7 for some aspects and TRL 8 for reproducibility of data. This team is the first to create the capability for accurate, real time physical measurements of the volume during semi-contained ISB. Creating the ability to directly measure the volume of burning oil in a semi-contained burn is a significant accomplishment for the BSEE and the spill response community. Advances were made in both the algorithm automation and the hardware integration. In addition to the advancements in technology we performed 65 burns with multiple replicates and quantified the burn rates and efficiencies in multiple ways for HOOPS, Alpine, and Rock for fresh and emulsified oils. The data show that one cannot simply assume a uniform burn rate over time for these burns since that approach overestimates the burn rate of the oil. These results advance the technology to enable BSEE and the spill response community to directly measure the volume of oil in the water and the instantaneous burn rates.

8. Future Work

Integrating these real-time area and thickness measurements into a single system and deploying it for large scale burns and in the open water will realize this capability for BSEE and the spill response community. A schematic of the integrated system is shown in Figure 60. The next steps include large scale burns were the oil is free to float or be semi-contained so that boil over can be avoided or studied if needed. The oil control and containment methods will enable direct comparison between burn rates and efficiencies over a large length scale. Integrating the thickness and area results into ERMA is a natural next step that can occur as well.


Figure 60.   Schematic of integrated SB measurement system.

9. References

1.   Panetta, P. D., Byrne, R., & Du, H. The Direct Quantitative Measurement of In-Situ Burn (ISB) Rate and Efficiency, AMOP 2017
2.   Panetta, P. D., Byrne, R., & Du, H. (2017, May). The Direct Quantitative Measurement of In-Situ Burn (ISB) Rate and Efficiency. In International Oil Spill Conference Proceedings (Vol. 2017, No. 1, pp. 1006-1019). International Oil Spill Conference.
3.   Panetta, P. D., Byrne, R., & Du, H. (2018). Quantitative Measurement of In-Situ Burn (ISB) Efficiency and Rate. (Bureau of Safety and Environmental Enforcement Oil Spill Response Research Project # 1074). https://www.bsee.gov/sites/bsee.gov/files/research-reports//1074aa.pdf
4.   Panetta, P. D., McElhone, D., Carr, L., & Winfield, K. (2015). Acoustic Tool to Measure Oil Slick Thickness at Ohmsett, Report For US Department of the Interior Bureau of Safety and Environmental Enforcement (BSEE), Project 1028, 2015
5.   Paul D. Panetta, Ted Argo, Hualong Du, Donglai, Gong, L.N. Ferris, and Jeanna Kidwell, Development of acoustic methods to measure oil droplet size and slick thickness on ROV and AUV platforms, Report For US Department of the Interior Bureau of Safety and Environmental Enforcement (BSEE), 2017.

10. Appendix

The burn rate and efficiency of the ISB were calculated from the volume of oil as a function of time based on direct measurements of the area and the thickness. A graphical representation of the algorithms used to determine the slick area and slick thickness as well as the resultant volume, burn rate, and efficiency are shown in Figure 61. The details of the algorithms and intermediate and final results are shown in previous sections of this report and the cited reports and publications.
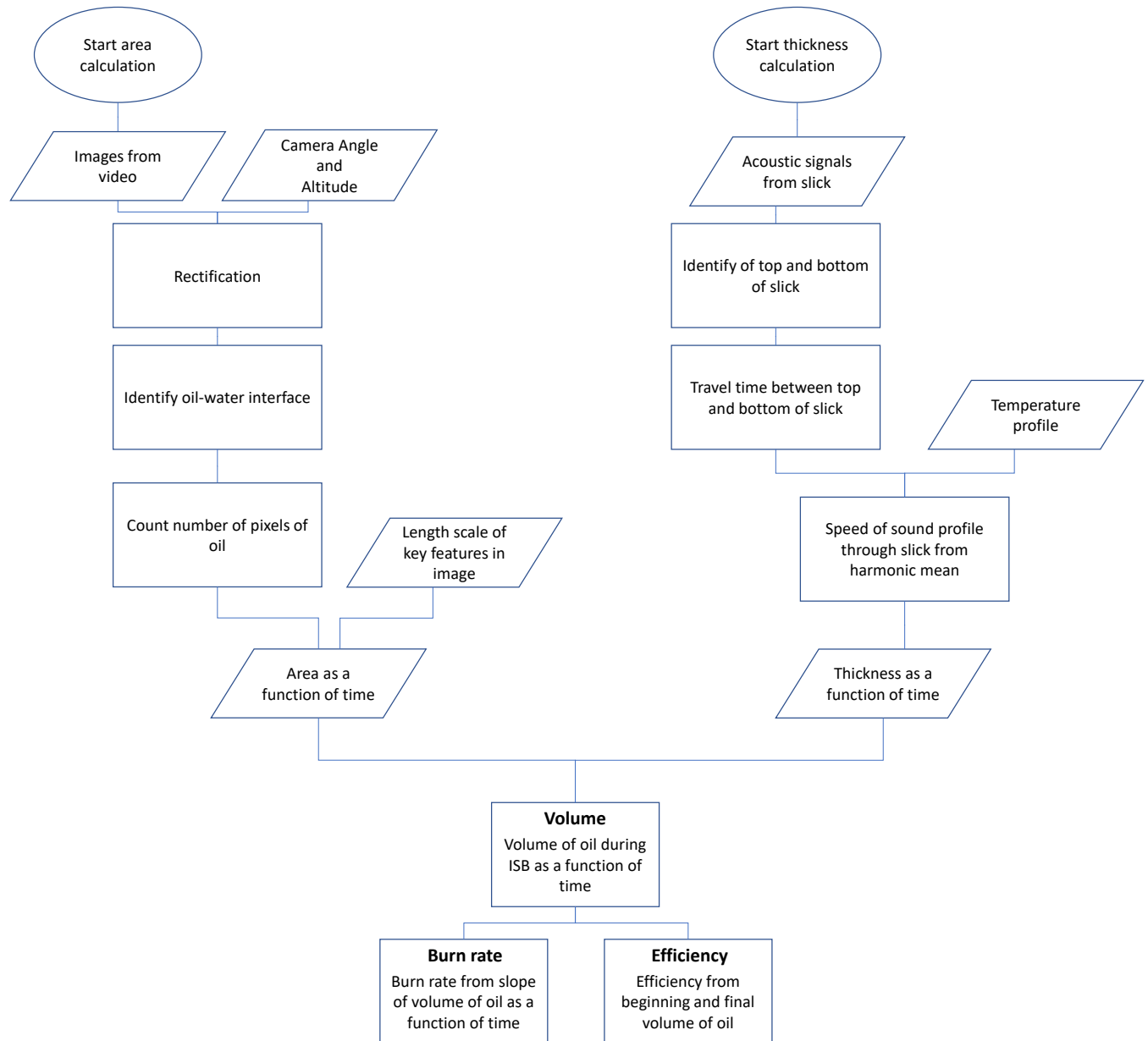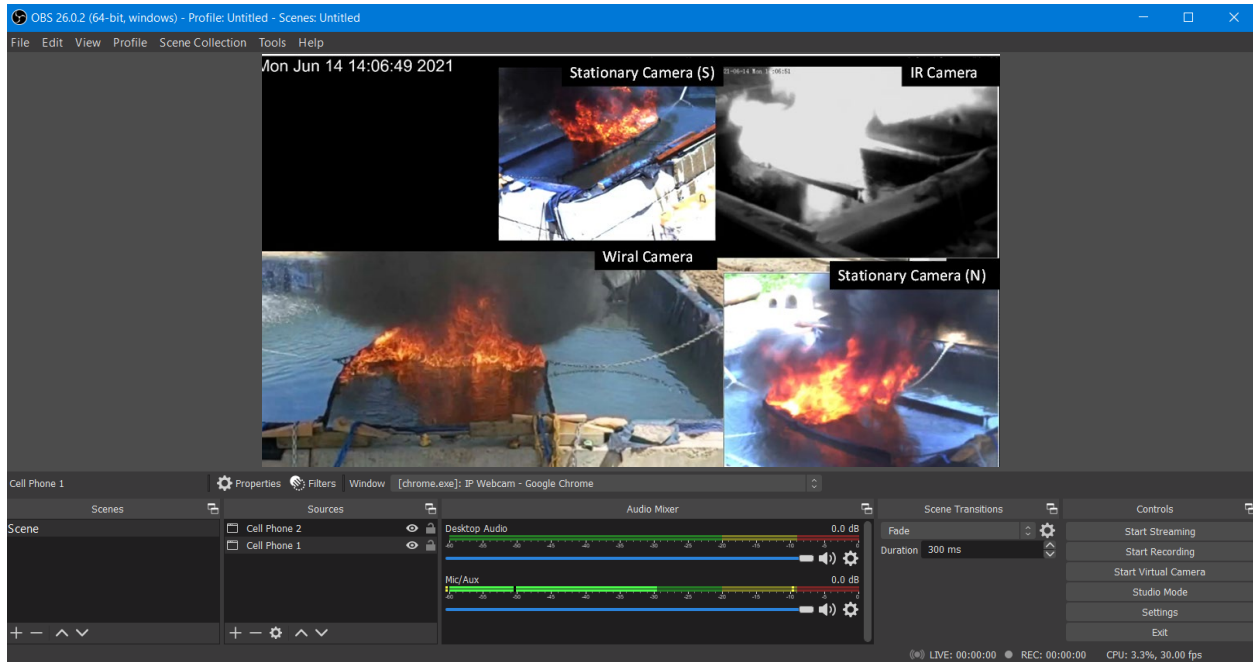

Figure 61. Graphical presentation of the algorithms used to calculate the slick area, slick thickness, resultant volume and subsequent burn rate and efficiency.
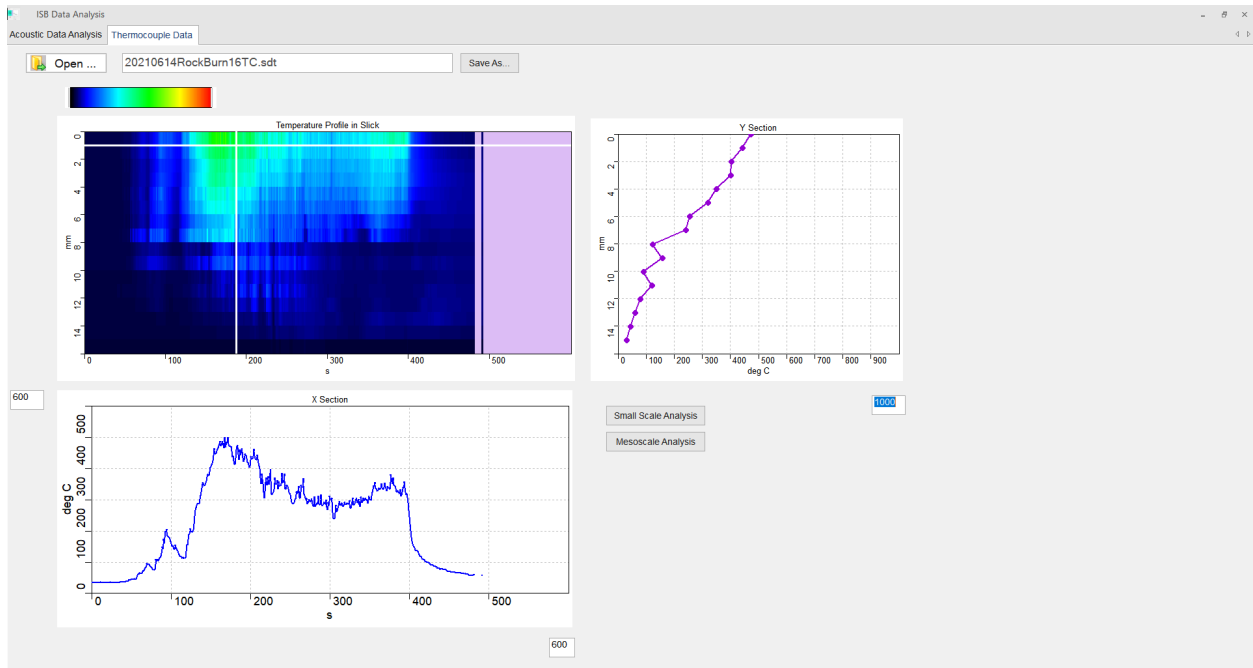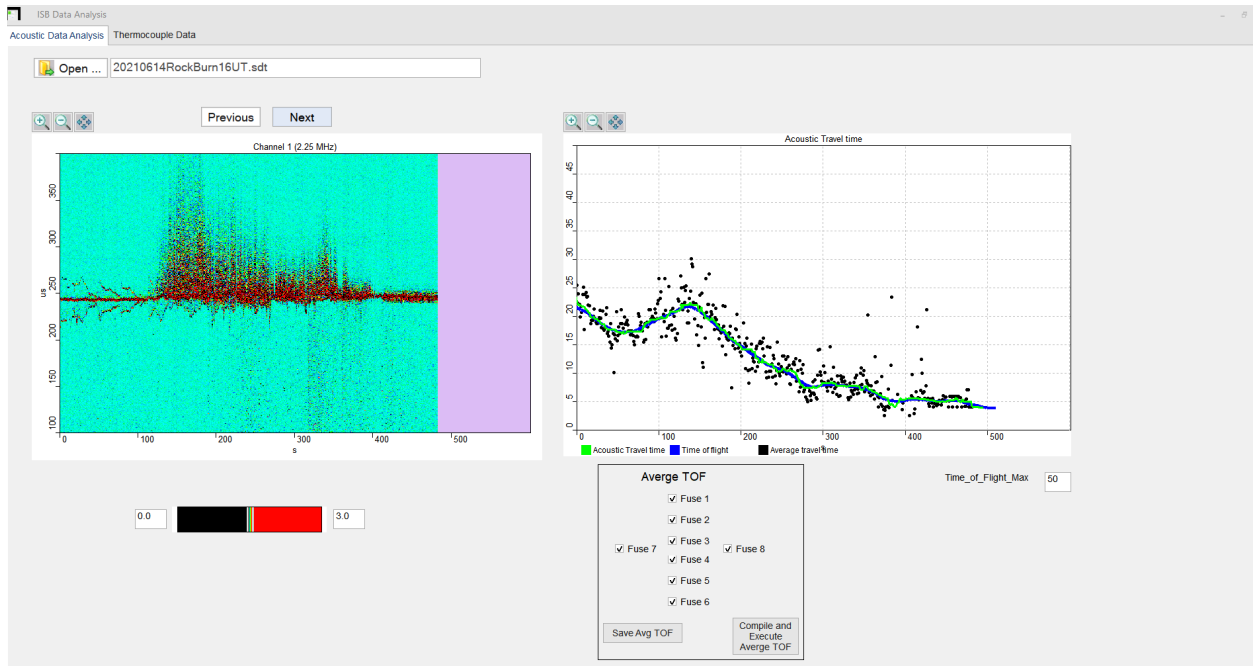
The user interface for the data acquisition and analysis for use by the team is shown in Figure 62, Figure 63, and Figure 64.
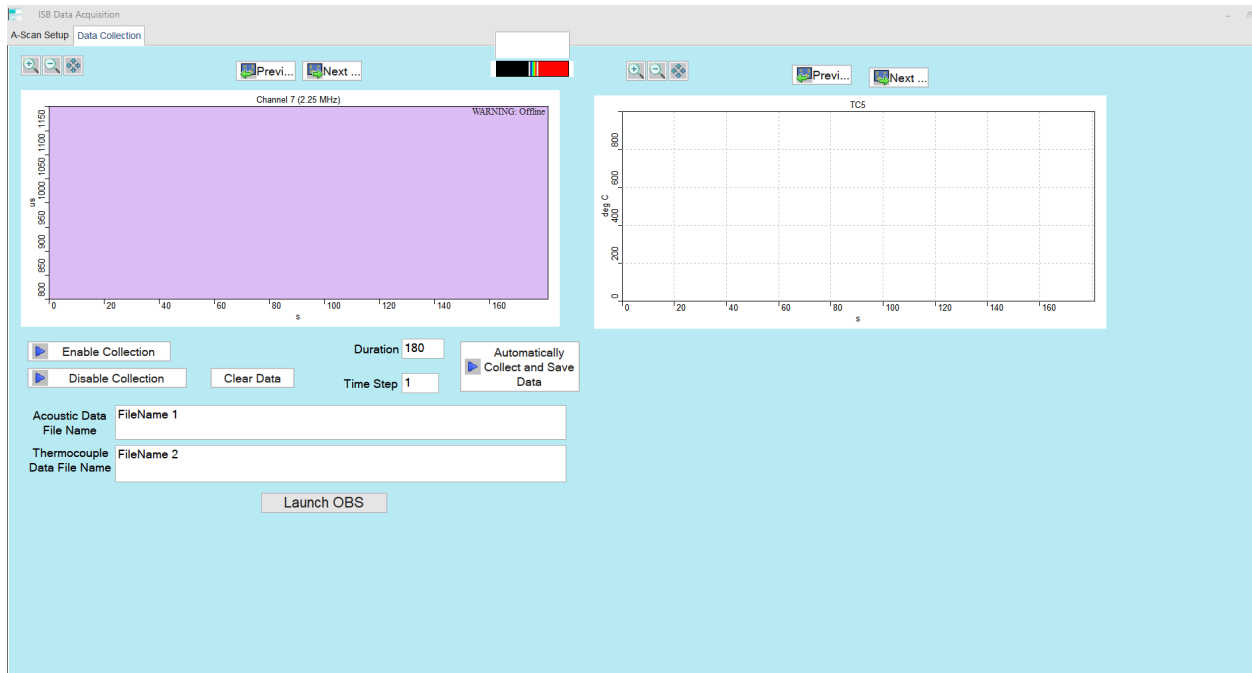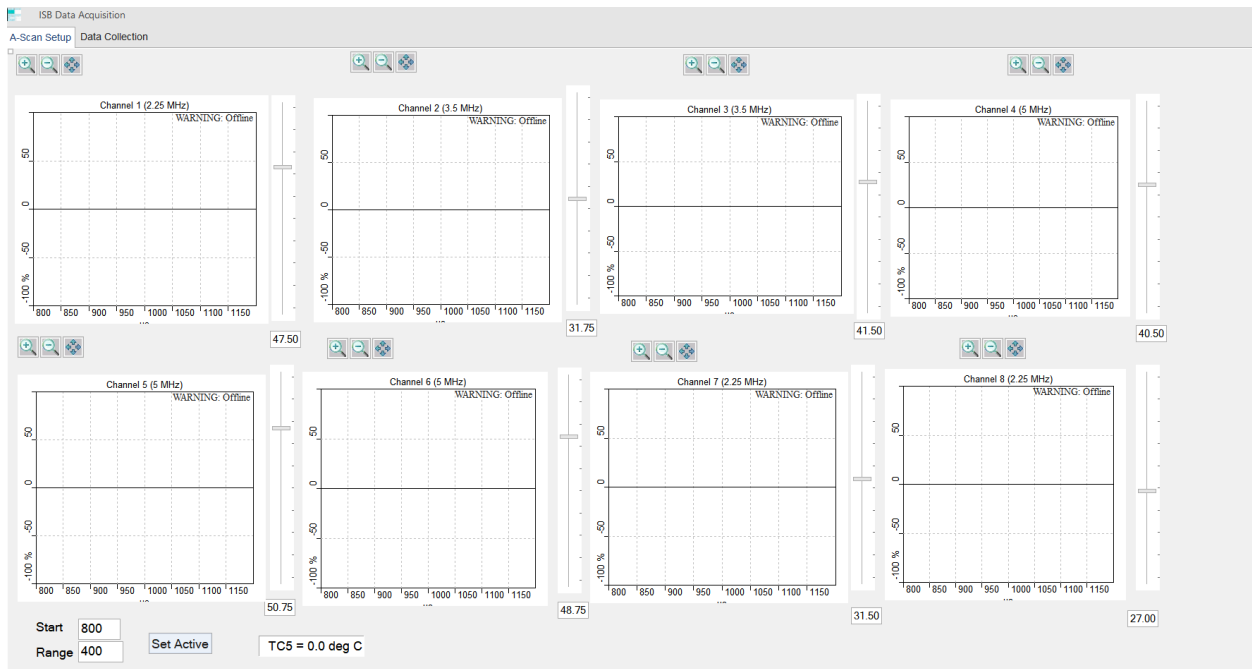
Figure 62. Data acquisition interface programed in InspectionWare software.

Figure 63. Video acquisition software using Open Broadcaster Software (OBS).

Figure 64. Data analysis interface programed in InspectionWare software.